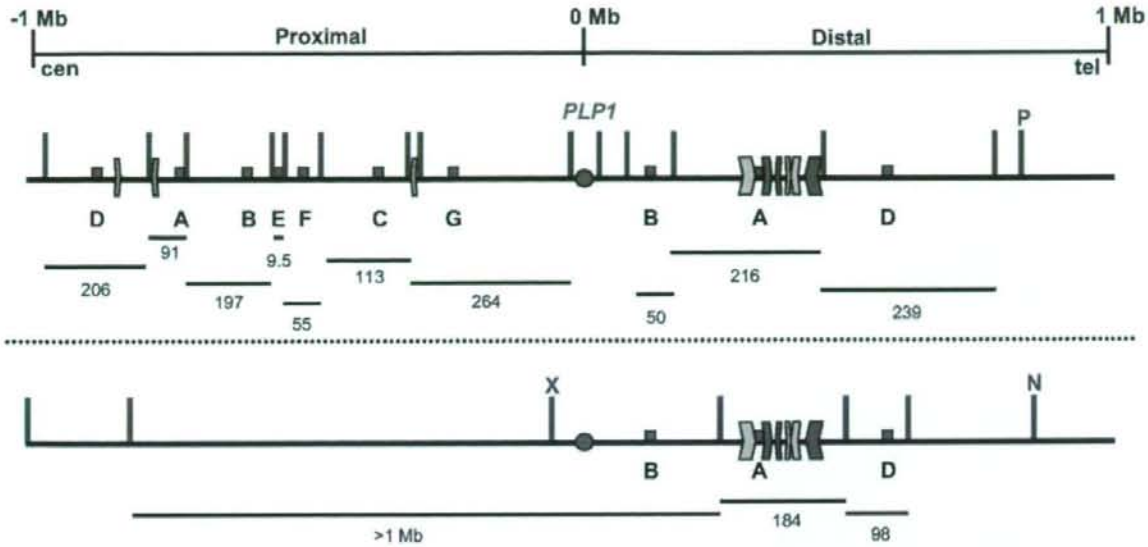

Figure 5. Probes adjacent to LCRs detect apparent junction fragments. Block arrows proximal to *PLP1* (red circle) centromeric (cen) to telomeric (tel) represent LCR–PMDE1, F5 and E2, respectively, which were identified by large-scale genome sequence analysis as described. Block arrows distal to *PLP1* include LCR–PMDA and B in dark blue and light blue, respectively, which are flanked by LCR–PMDC (yellow) and LCR–PMDD (dark green). Proximal A through G probes were designed proximal to *PLP1*, whereas the Distal A, B and D probes were designed distal to *PLP1*. The positions where probes hybridize are shown as small red squares. The upper and lower panels depict the restriction maps for enzymes *Pme*I, 'P,' and *Nru*I, 'N,' respectively. The expected band sizes by Southern hybridization with a particular probe and restriction enzyme combination are specified in kilobases below each restriction map. 'X' indicates that *Nru*I does not cut at the expected site, likely because of its CpG methylation sensitivity. Positions are given relative to the *PLP1* gene in megabases.

Table 3. Summary of band sizes (in kb) observed for *PLP1* duplication patients tested for hybridization with Proximal B, C, and G and Distal A probes

Family	Patient	Proximal B probe		Proximal C probe		Proximal G probe		Distal A probe	
		*Pme*I	*Nru*I	*Pme*I	*Nru*I	*Pme*I	*Nru*I	*Pme*I	*Nru*I
HOU587	BAB1482	197	ND	113,136	*480*	264,*375*	*480*	216,*375*	184,*480*
	BAB1597	197	ND	113,136	*480*	264,*375*	*480*	216,*375*	184,*480*
HOU519	BAB1334	197	ND	113,136	ND	264	ND	216,*375*	184
HOU674	BAB1705	197	ND	ND	ND	264	ND	216,*295*	184,*400*
	BAB1707	197	ND	ND	ND	264	ND	216,*295*	184,*400*
HOU503	BAB1305	197	ND	113,136	ND	264	ND	*295*	*100*
HOU501	BAB1301	197	ND	113,136,*190*	ND	264	ND	216	ND
HOU486	BAB1261	197	ND	113, 115,*127*,136	*650*	264	*650*	*275*	*100*
HOU494	BAB1282	197	ND	*90*,113,*115*,136	*650*	264	*650*	216,*275*	*100*,184
HOU491	BAB1275	197,*210*	ND	113,136	ND	264	ND	216	ND
HOU497	BAB1290	197	ND	113,136	ND	264	ND	216,*295*	*100*,184
HOU561	BAB1420	197	ND	ND	ND	264	ND	*295*	*100*

Hybridization with all other probes in the probe series yielded expected band sizes. Band sizes in italics indicate approximate junction fragment lengths; all others indicate observed bands of expected sizes. 'ND' signifies not determined. All band sizes listed are estimated based on migration with a yeast or lambda DNA size marker.

normal bands after *Nru*I digestion, indicating that for the junction fragment, the *Nru*I sites flanking the hybridization probe are closer together than on non-rearranged DNA. By restriction analysis for family HOU494, the duplication is consistent with being directly oriented, but appears to be interrupted, and inserted nearby the original reference sequence. Interestingly, we observed the absence of bands of expected sizes based on restriction maps in family HOU486, and also in families HOU503 and 561, and instead saw junction fragments only, suggesting that more complex rearrangements have occurred, and that more than one breakpoint may have occurred within the same restriction fragment. For families HOU486 (BAB1261) and HOU503 (BAB1305), the distal breakpoints determined by PFGE align with that found by array CGH analysis. However, for family HOU561 (BAB1420), array CGH analysis detected a duplication that extends three more BAC clones (~500 kb) distal to that predicted by PFGE analysis, also consistent with a complex rearrangement. We detected no bands for family member BAB1698 (HOU486) for hybridization with

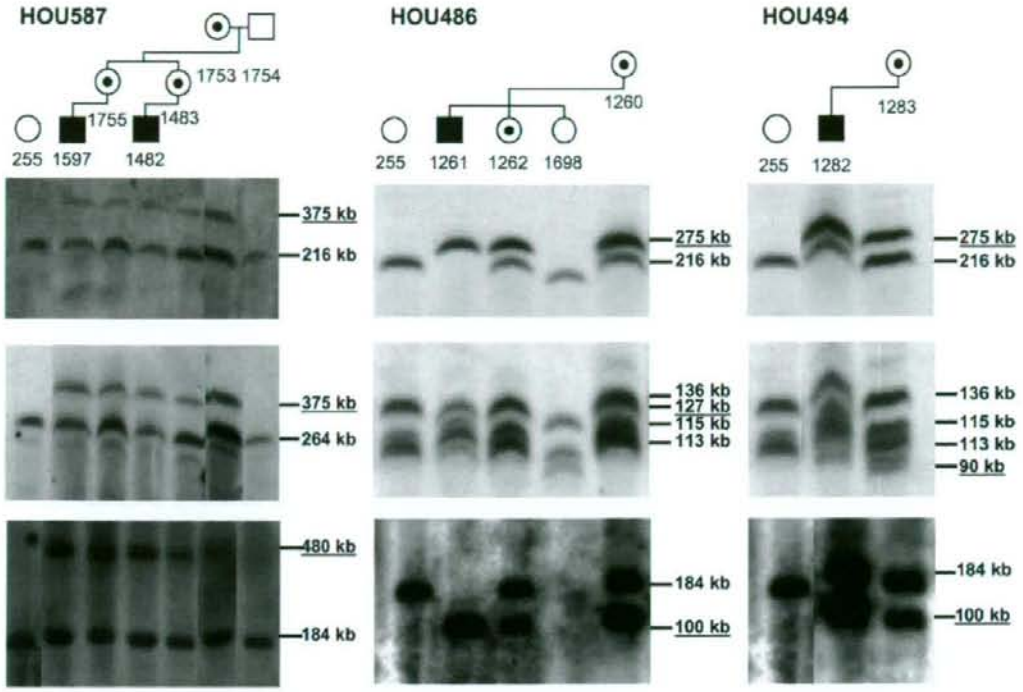

Figure 6. Junction fragments segregate in families. Shown are the PFGE data for *Pme*I and *Nru*I digestions. Family HOU587 is shown on the left, family HOU486 in the center and family HOU494 on the right. Hybridization with Distal A probe after *Pme*I digestion is shown in the first row, and after *Nru*I digestion in the last row for all three families. In the second row, hybridization with Proximal G probe after *Pme*I digestion is shown for family HOU587, whereas hybridization with Proximal C probe after *Pme*I digestion is shown for families HOU486 and 494. Approximate band sizes are shown in kilobases to the right of each blot. Junction fragments (band sizes underlined) are identified as bands of sizes differing from those observed for the control individual (BAB255).

the Distal A probe after *Nru*I digestion, which is possibly due to mutation affecting the *Nru*I restriction pattern in this individual, as bands are otherwise able to be visualized by hybridization with other probes. A summary of the results of our PFGE analysis of patients in families HOU587, 486 and 494 is illustrated in Figure 7, highlighting LCR–PMDE2 found adjacent to where Proximal C and G probes hybridize, and LCR–PMDA found adjacent to where Distal A probe hybridizes.

Diverse duplication breakpoints with grouping near complex genomic architecture supported by recombinant junction analysis

Earlier, we showed by array CGH that duplications have diverse breakpoints, but that they occur in groups coincident with LCRs. Furthermore, in a prospective approach, we used unique sequence probes adjacent to LCRs in Southern analysis, after separation of high molecular weight genomic DNA by PFGE, to detect junction fragments associated with the rearrangement breakpoints. To examine an independent data set to determine whether or not there was any evidence for grouping among the diverse breakpoints, we utilized the recently published PMD duplication recombinant junction sequence analysis by Woodward *et al.* (19). This enabled us to position *PLP1* duplication breakpoints precisely on the X chromosome genomic sequence to examine for breakpoint grouping and potential association with LCRs. Indeed, we found an apparent grouping of breakpoints coincident with LCRs (Fig. 8). In fact, ~62% of the proximal breakpoints (8/13) and ~79% of the distal breakpoints (11/14; one patient has two sequenced distal breakpoints) occur within or near LCR-containing BAC clones. Overall, ~77% of patients (10/13) in their data set had at least one breakpoint within or near an LCR-containing BAC clone. In common, with our subset of patients with at least similar breakpoints at a BAC/PAC resolution, the proximal breakpoints of their data set (6/13 patients) occurred within or near BAC clone RP11-1123D8 (LCR–PMDE2), and the distal breakpoints of their data set (9/13 patients and 3/13 patients) occurred within or near BAC clones RP11-34P3 (LCR–PMDC) and RP11-462K21 (LCR–PMDA, B, and D), respectively. In addition, two of their patients had proximal breakpoints within or near BAC clone RP11-155E24 (LCR–PMDE1).

The duplications are directly oriented

The PFGE restriction patterns we observed for families HOU486, 503 and 561 prompted us to investigate duplication orientations in all available patients. Two-color FISH analysis

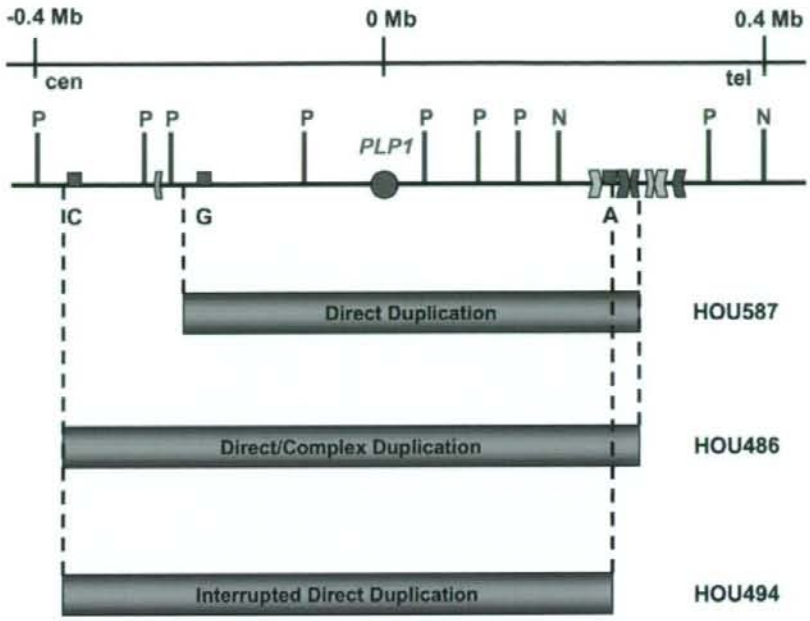

Figure 7. PFGE junctions map breakpoints near LCRs. Summary view of *PLP1* duplications found in families HOU587, 486 and 494 by PFGE analysis; duplications are shown as pink horizontal bars. Positions of the Southern hybridization probes (red squares) relative to the LCR–PMDs most nearby the duplicated regions are indicated. LCR–PMDE2 (light green) is the nearest LCR adjacent to Proximal C and G probes (~31 and ~33 kb away, respectively). LCR–PMDA (dark blue), B (light blue), C (yellow) and D (dark green) are shown distal to *PLP1* (red circle). LCR–PMDA is the nearest LCR to Distal A probe (<20 bp away). Restriction sites for *PmeI* digestion are shown as 'P' (purple) and for *NruI* as 'N' (blue). The approximate endpoints of the duplications are specified by the dashed lines. Duplications are displayed for each family as direct, direct/complex and interrupted direct.

for each patient revealed an alternating red-green-red-green signal order consistent with directly oriented duplications in patients BAB1305, 1301, 1261, 1282, 1275, 1290, 1420, 2389, 2390, 2396 and 2425, as had been observed previously (14). For patients BAB1482, 1597, 1334, 1705 and 1707, the furthest duplicated clones, RP11-1144F22 and RP11-34P3, had only 51 kb of genomic sequence between them, and thus the fluorescent signals could not be reliably distinguished by interphase FISH. Representative data for the direct duplications are shown in Figure 9. For all unaffected male and female control chromosomes, we observed only a red-green signal pattern (data not shown).

No evidence for an association with copy-number variation in LCR–PMDA and B region

We previously identified copy-number variation (CNV) within the LCR–PMDA and B region within a Caucasian control population by a quantitative real-time PCR assay (29). We sought to determine if our PMD patients or family members have CNV in this region in order to investigate CNV as a potential further genomic susceptibility factor for rearrangements. Using the same quantitative real-time PCR assay (29), we evaluated all available PMD patients and family members for CNV in the LCR–PMDA and B region. The results of our dosage assay (data not shown) were consistent only with either *PLP1* duplication or duplication carrier status, and were consistent between patient and mother, as determined previously by FISH and PFGE analyses. Thus, there was no evidence for CNV in the interrogated region in this cohort of patients and family members. These real-time PCR results were also informative for breakpoint analysis in some patients, allowing us to either include or exclude the interrogated region as duplicated or not duplicated, respectively (data not shown).

DISCUSSION

PLP1 duplications causing PMD have been reported as varying in size with scattered breakpoints and lack of homology reported at the actual breakpoints (14,30). For both *PLP1* deletions and duplications causing PMD, recombinant junction sequence analysis revealed a lack of homology and the addition of nucleotides at the breakpoints, consistent with recombination occurring by an NHEJ mechanism (18,19,31). Moreover, NHEJ has been implicated recently as an alternative mechanism responsible for a number of human genomic disorders because of non-recurrent rearrangements with scattered breakpoints (22,23,32). On the basis of the following observations, we suggest that the LCRs not only render this genomic region unstable and susceptible to

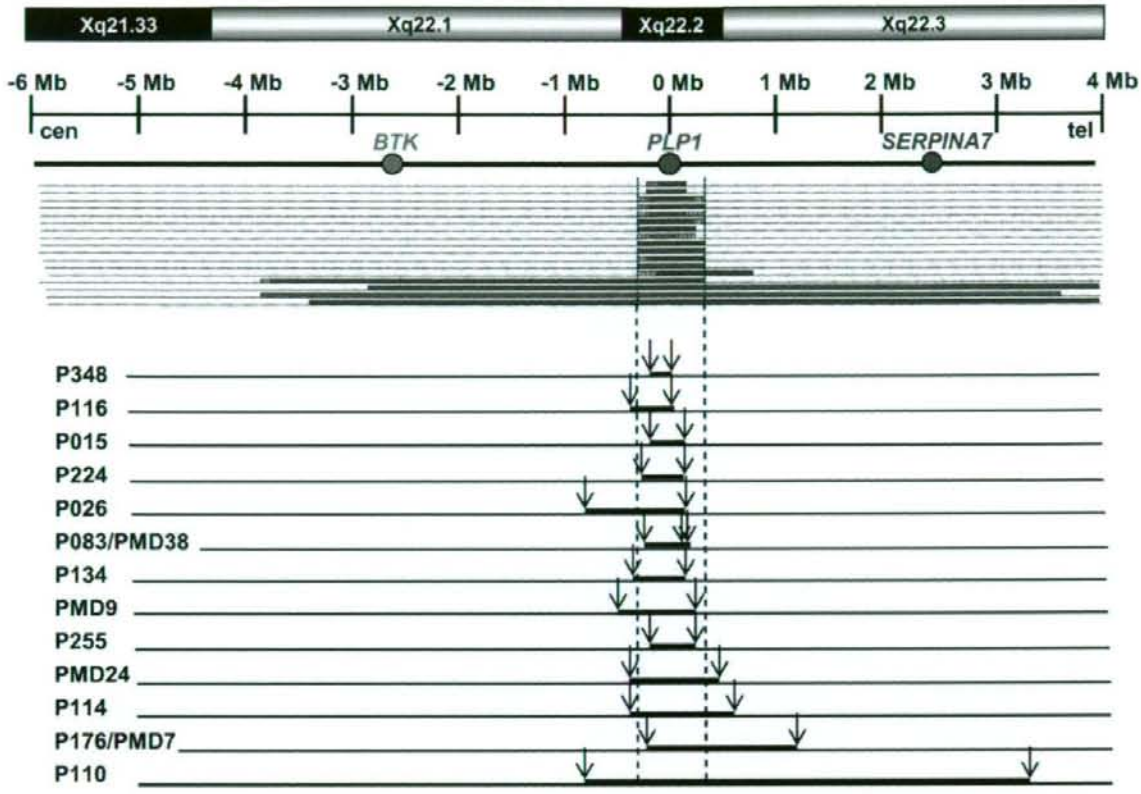

Figure 8. Comparative analysis of an independent data set (19) reveals apparent grouping of breakpoints. The region detected by array CGH is shown on the top, followed by the duplications found in our patients by array CGH in condensed form (Fig. 3). Below are the duplications reported by Woodward *et al.*, and their alignment within our ~10 Mb array detection region. For this independent data set, patients are shown on the left; duplication breakpoints are shown as vertical arrows, whereas the duplicated segments are shown as bold black lines between the arrows. Similar breakpoint regions in a subset of our patients are delineated by vertical dotted lines.

rearrangements, but that they are in fact, stimulating these genomic rearrangements.

Genomic architecture of the *PLP1* region is complex

By *in silico* genome sequence analysis, there is no gap in sequence information between LCR–PMDA and B, unlike what we previously published based on the then current draft sequence information. According to our FISH mapping data (14), the distal breakpoint ends of *PLP1* duplications in most *PLP1* duplication families tested grouped at or near LCR–PMDA and B, a complex arrangement of four LCRs of varying shared sequence identities and different relative orientations (Figs 1 and 2; Table 1), whereas the proximal breakpoints were more scattered. These data prompted us to perform an extensive *in silico* genome sequence analysis described herein that uncovered many LCRs scattered proximal to *PLP1*, and fewer distal to *PLP1*. Interestingly, the locations of scattered LCRs within 2.3 Mb of sequence proximal to *PLP1* correlates with the scattered proximal breakpoints previously reported in *PLP1* duplication patients, and the clustering of LCRs distal to *PLP1* correlates with the grouped distal breakpoints previously reported (Fig. 1).

LCR–PMDs are associated with duplication breakpoints in a subset of patients

Although duplication breakpoints proximal to *PLP1* have been shown to be scattered, array CGH analysis on our cohort of *PLP1* duplication patients surprisingly revealed that there is a subgroup of duplication patients who have similar proximal and/or distal breakpoints at a BAC/PAC resolution (Figs 3 and 4), accounting for ~71% of our patient cohort (15/21) or 71% of families (12/17). Furthermore, when our array CGH breakpoint mapping data were aligned with LCR data generated from *in silico* analysis, we found that the breakpoints in 12 families aligned with the locations of LCR–PMDs with statistical significance

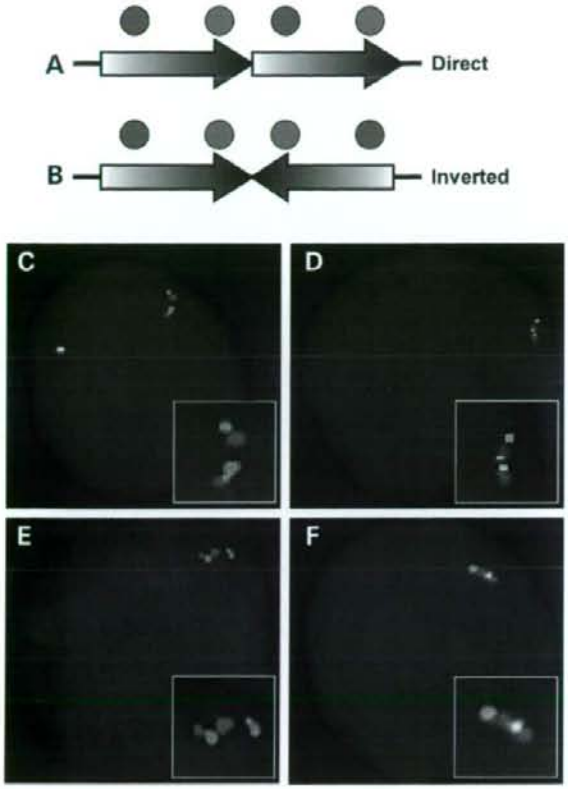

Figure 9. FISH showed direct orientation of duplications. Representative data for two-color FISH analysis for duplication orientation are shown. The signal order is shown as (**A**), red-green-red-green for direct duplication and (**B**), red-green-green-red for inverted duplication. The BAC probe labeled in red is the most proximal fully duplicated clone (if available), whereas the BAC probe labeled in green is the most distal fully duplicated clone (if available) as shown by array CGH. (**C**) shows a representative analysis of the mother of a male duplication patient, whereas (**D**–**F**) show representative orientation analyses of unrelated male duplication patients. Enlargements of the duplicated segments are shown in each respective insert. These data are typical results for the direct duplications we observed.

($P = 1.255 \times 10^{-5}$). In fact, for this subgroup, we found that 92% of their proximal breakpoints and 92% of their distal breakpoints occur within LCR-containing BAC clones or duplication end-clone pairs.

By PFGE analysis, we were able to confirm that the LCRs in the *PLP1* region are associated with breakpoints of duplications causing PMD. Using probes that map in proximity to LCRs and target suspected proximal and distal breakpoint regions, we identified junction fragments in 12 patients in 10 families; in four of them, junction fragments were identified on both the proximal and distal ends of the duplicated segments. These four patients are included in the subgroup of patients who have similar proximal and distal breakpoints at a BAC/PAC resolution. The Distal A hybridization probe, designed adjacent to LCR–PMDA and B, detected distal junction fragments in the majority of patients tested, whereas multiple hybridization probes mapping proximal to *PLP1* were informative, consistent with the pattern of LCRs we find in this region. In other words, a majority of distal breakpoints occur near or within LCR–PMDA and B in our patients, whereas the proximal breakpoints occur near various LCR–PMDs. Junction fragments could not be resolved for patients with particularly large or small duplications under the separation conditions and by the restriction enzymes used. In addition, if a duplication proximal breakpoint occurred within LCR–PMDE2 or within the 9.5 kb between the *Pme*I sites flanking LCR–PMDE2, the resulting junction fragment would only be able to be detected after *Nru*I digestion, unless conventional Southern analysis were performed. Our PFGE data presented herein suggest an association between breakpoints and proximal and distal LCRs, implicating genome architecture in the rearrangement events leading to *PLP1* duplications in some PMD patients.

Moreover, when we investigated the potential grouping of breakpoints in an independent data set published by Woodward *et al.*, in which recombinant junctions were sequenced (19), we also found that indeed a majority (10/13) of their patients had at least one breakpoint within or near LCR-containing BAC clones. In particular, similar to the findings reported herein, we found an association between LCR–PMDE1 and E2 and proximal breakpoints, and between LCR–PMDA, B, C, and D and distal breakpoints in their data set.

PLP1 duplications may share a common mechanism

PLP1 duplications resulting in PMD generally occur in tandem by an intra-chromosomal event in an ancestral male during gametogenesis (14,21,33). Intra-chromosomal events having occurred in an ancestral male are also responsible for duplications causing Duchenne muscular dystrophy (34) and *PLP1* deletions (18).

In analyzing PFGE data, the placement of hybridization probes relative to the restriction sites can be informative for determining breakpoint locations of rearrangements (35). By PFGE analysis, we observed similar size-junction fragments for some unrelated patients, possibly indicating that they share a common breakpoint region, or at least that the breakpoints occur within a similar genomic vicinity. Our array CGH analysis revealed that the breakpoints are indeed similar for a subset of patients. Also, our restriction analysis by PFGE showed that the rearrangements in some of our patients are consistent with directly oriented duplications. Likewise, our two-color FISH analysis revealed that the duplications in all patients tested were direct in orientation. The commonalities observed in the junction fragment sizes, breakpoint locations and duplication orientations suggest that a common mechanism may be responsible for the duplication rearrangements in these patients.

The *PLP1* region is prone to rearrangement

Not only have patients with PMD resulting from *PLP1* duplication, deletion or point mutations been described, but other DNA rearrangements have also been shown to be causative. PMD cases in which *PLP1* has behaved as a sub-microscopic

transposon have been reported (30,36), including one in which all the genetic material including the centromere was inverted between two intact *PLP1* copies (30). Whether inversions are the cause of such duplications, or if duplications have led to these inversions by mispairing is difficult to determine. In addition, extra copies of *PLP1* have been reported to be found on some autosomes (18,37). Interestingly, in some patients, three or more copies of *PLP1* have been reported (38), including partial triplications and partial deletions as well (39). We report herein at least one patient (BAB1282) with an interrupted direct duplication, and at least three patients (BAB1305, 1261, 1420) with potentially complex duplication rearrangements as shown by the absence of normal-sized bands by PFGE analysis, one of which (BAB1420) has a duplication detected by array CGH that extends three more BAC clones (~500 kb) distal to that predicted by PFGE analysis. Considering that the region surrounding *PLP1* contains numerous LCRs based on *in silico* analysis reported herein, and that repeat sequence confers genome instability (1,40), the genomic architecture likely renders the DNA in this region highly susceptible to duplication and other rearrangements causing PMD.

Particular LCR–PMDs may be hotspots for stimulating *PLP1* duplications

It appears that the region containing LCR–PMDA and B is possibly a hotspot for stimulating rearrangements (18), including those leading to CNV of the LCR–PMDA and B region in normal individuals as we recently described (29). CNV in the LCR–PMDA and B region was excluded in this study, in all available PMD patients and family members. Besides LCR–PMDA and B, LCR–PMDE2, which is the closest LCR proximal to the *PLP1* gene and is adjacent to PFGE Proximal C and G probes (Fig. 5), may also play a role in stimulating *PLP1* duplication events, as we report rearrangement proximal breakpoints having occurred near this sequence. Therefore, we suggest that rearrangements stimulated by both of these particular LCR regions together, proximally and distally, in the same event result in duplications of relatively similar size in some patients. Likewise, other pairs of LCRs in this region may stimulate rearrangement together, proximally and distally, in other PMD patients, resulting in the various sizes of *PLP1* duplications that we observe. The underlying genomic architecture may also be responsible for the grouping of similar duplication size superimposed on the diversity, perhaps reflecting apparent breakpoint-prone genomic regions.

Model for *PLP1* duplication rearrangements

We suggest that LCR–PMDs may be hotspots for stimulating rearrangements, possibly by acting together in the same rearrangement event, and thus render the DNA surrounding the *PLP1* gene unstable and susceptible to rearrangements causing PMD. Interestingly, although most *PLP1* duplications have been reported to be oriented head-to-tail in tandem, we report three potentially complex rearrangements and one interrupted duplication which appears to be inserted near the original reference sequence. Similarly, *PLP1* duplications have been reported to act sometimes as transposons (30,36). We propose a general model (Fig. 10), which incorporates the following: the role of LCR–PMDs in rendering the DNA susceptible to double-strand breaks (DSBs), a mechanism of coupled one-sided homologous single-strand invasion and repair by NHEJ. This model can explain duplications and deletions as well as intra- and inter-chromosomal transposition of the duplicated *PLP1* segment and complex rearrangements.

In this model (Fig. 10), the rearrangement originally occurs during gametogenesis in the ancestral male (33). We propose this event occurs by the induction of a single DSB stimulated by a nearby LCR–PMD. Much like long tract gene conversion (LTGC) (41), and as recently discussed by Woodward *et al.* (19) in the context of *PLP1* duplications, a one-sided single-strand invasion by the broken chromatid occurs in which the sister chromatid is copied. Consistent with what has been found for other *PLP1* duplications (19) and deletions (18), this event is completed by a NHEJ repair mechanism (42).

However, for the cases in which the duplicated segment becomes transposed and inserted either intra-chromosomally, such as the case of interrupted direct duplication inserted close by which we report herein, or inter-chromosomally to autosomes or the Y chromosome, we propose that a second DSB may be stimulated by another nearby LCR–PMD in *trans*, followed by transposition of the duplicated segment to a secondary chromosomal location and repair by NHEJ. Furthermore, our model may also help to account for some complex *PLP1* duplication rearrangements (19), for which more than one proximal or distal breakpoint is predicted. These rearrangements may be explained by part(s) of the duplicated segment being deleted and/or inserted, in a direct or inverted orientation, at either the primary rearrangement site or elsewhere in the genome. For such rearrangements, we hypothesize that at least two LCR–PMDs stimulate at least two DSBs, or potentially greater than two in more complex rearrangements, breaking the duplicated segment into fragments that may become either lost or integrated by NHEJ either intra- or inter-chromosomally, conceivably in inverted or direct orientations and not necessarily in tandem.

CONCLUSIONS

We illustrate that the genomic architecture of the region surrounding *PLP1* is complex, as it contains numerous LCR–PMDs, especially proximal to *PLP1* (Fig. 1). Our data suggest that genomic architectural features, namely LCRs, may stimulate although not necessarily mediate the genomic rearrangements responsible for the majority of PMD cases, as LCRs were identified near the breakpoint regions in a majority of our patients. Specifically, genomic architecture may play an important role in rendering DNA in the *PLP1* region more susceptible to rearrangement, resulting not only in duplications of varying size, but also in the grouping of some duplications of apparently similar size. Duplication rearrangements may be quite common in the human genome; however, only when they result in ascertainable

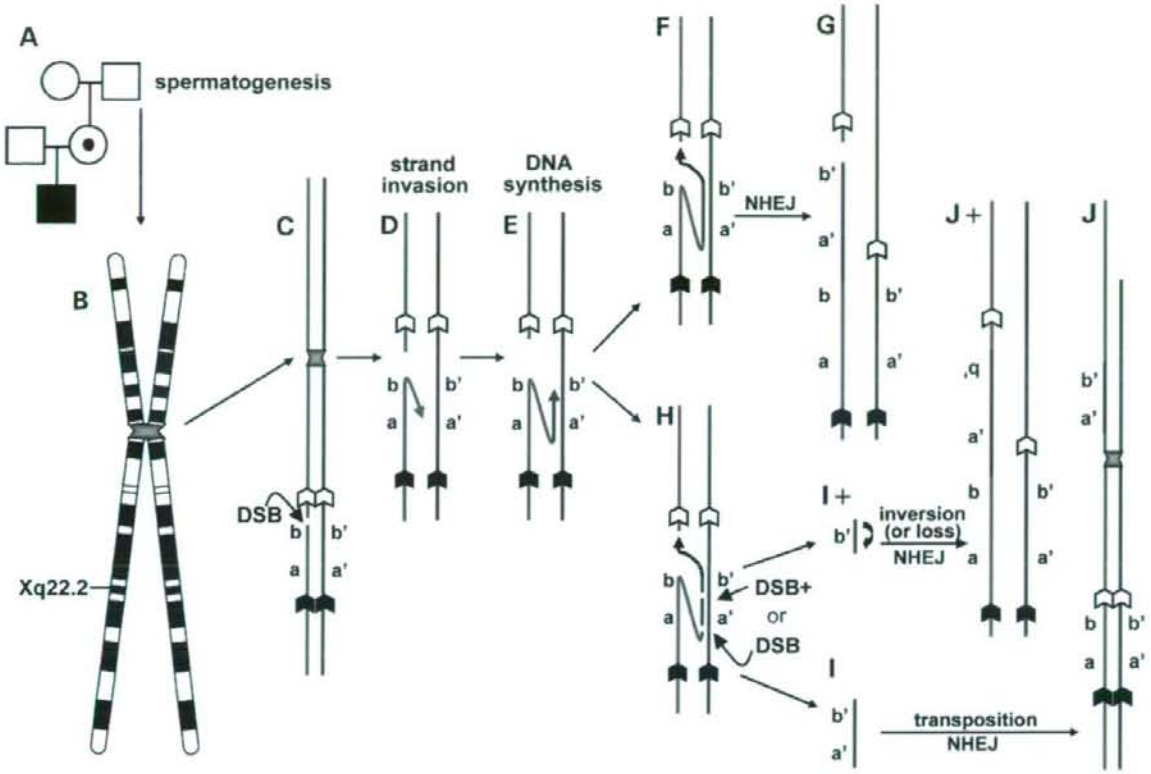

Figure 10. General model for *PLP1* duplication rearrangements. (**A**) The rearrangement originally occurs during spermatogenesis in the ancestral male on his X chromosome, shown as an ideogram in (**B**). (**C**) A DSB is induced near an LCR–PMD (open block arrow). This is followed by (**D**), a strand invasion by the blue chromatid, and (**E**), DNA synthesis off the maroon chromatid template. From here, two pathways can emerge. (Top) (**F**) After DNA synthesis, the chromosome is repaired by NHEJ (**G**). (Bottom) (**H**) A second DSB is induced in *trans* near another LCR–PMD (filled block arrow) at the proximal end of the duplication rearrangement, followed by (**I**), transposition of the duplicated segment and (**J**), repair by NHEJ. (**I+**), Alternatively, DSBs can be induced in *trans* in the middle of the duplication rearrangement, breaking it into segments, which could become inverted (curved arrow) before becoming integrated into the broken chromatid as shown, or which may become lost. (**J+**), repair is completed by NHEJ. Loci are shown as **a** and **b** on the original blue chromatid, and **a'** and **b'** correspondingly on the original maroon chromatid. Segment containing loci **a'** and **b'** on the maroon chromatid is copied, and this copy either is incorporated into the blue chromatid in tandem as shown in (G) (top), or is transposed and incorporated intra-chromosomally, for example, as shown in (J) and (J+) (bottom). Inter-chromosomal transposition is also possible with this model.

human disease phenotypes are they likely to be discovered. *PLP1* duplication rearrangements causing PMD represent one example of many genomic rearrangements causing human disease that are stimulated by complex genomic architecture in the region surrounding the causative dosage-sensitive gene.

MATERIALS AND METHODS

In silico analysis of the *PLP1* region

To define the genomic architecture in the Xq22 region that potentially facilitates the variable *PLP1* duplication events, we performed *in silico* genome sequence analysis covering 8 Mb of repeat-masked DNA sequence from NCBI draft build 35 surrounding the *PLP1* region by BLAST 2 analysis using default parameters (http://www.ncbi.nlm.nih.gov/blast/bl2seq/wblast2.cgi) (43); DNA sequences were obtained from the UCSC Genome Browser (http://genome.ucsc.edu/) (44,45). Specifically, this analysis was performed by dividing the entire analyzed region into ~1 Mb segments; the sequence for each ~1 Mb segment was then compared with itself and with each of the other segments by BLAST 2 to identify LCR sequence and genomic architecture within the analyzed region. We compiled these LCR data from the present analysis together with LCR–PMDA through D (18,19). The sizes of the LCRs detected may be underestimated because each individual identity match does not include interspersed repetitive sequences and low complexity DNA sequences. Additional BLAST 2 analyses of breakpoint clones were performed to further assess for LCRs.

Patients

We obtained samples from 21 PMD patients with *PLP1* duplication and their family members (BAB#) in 17 families

(HOU#) after acquiring informed consent approved by the Institutional Review Board for Human Subject Research at Baylor College of Medicine. Most patients were ascertained because of leukodystrophy and molecular diagnostic evaluation for *PLP1* rearrangement mutations. Clinical details have been published elsewhere for the majority (Table 2). We established lymphoblastoid cell lines from peripheral blood lymphocytes by standard methods for all patients except for patients of BAB2448 and 2390. We performed FISH to confirm *PLP1* duplication status as described (14,46).

Custom array CGH

We prepared and printed DNA from either 38 or 68 BAC and PAC clones tiling an ~5 or ~10 Mb region surrounding *PLP1*, respectively, in addition to control clones from chromosomes 1, 2, 5, 10, 17, X and Y, as described (47). We isolated patient and control genomic DNA either by phenol/chloroform extraction from human cell lines or from peripheral blood using a Puregene kit (Gentra). We digested patient and control genomic DNA with *Dpn*II (New England Biolabs), labeled and hybridized the DNA, and then washed and scanned the slides as described (47). We combined dye reversal pairs for subsequent comparative analysis using a threshold of 0.2 on a log scale.

Pulsed-field gel electrophoresis

We harvested intact lymphoblastoid cells from PMD patient and control individuals and resuspended them in 1% InCert agarose (BMA). We digested DNA in agarose plugs from 5×10^6 cells with *Pme*I or *Nru*I restriction enzymes for 2 days at 37°C (New England Biolabs), followed by separation ranging from 10 kb to 1 Mb on a 1% agarose gel (Bio-Rad) in 0.5X Tris–Borate–EDTA buffer using a Bio-Rad CHEF Mapper. All samples co-migrated with a yeast or lambda chromosome size marker (New England Biolabs). We visualized separated DNA by ethidium bromide (Sigma) staining.

Probe design and preparation

We designed a series of DNA probes to target regions adjacent to the LCRs in the *PLP1* region revealed by *in silico* analysis. Also, we designed additional probes to obtain better coverage. Primer sequences for DNA probes proximal (centromeric) to *PLP1* include: Proximal A, 5′-AGATGTATTCCCTGCCCC ACTAC-3′ and 5′-GTAGCAAGTACAGAGCTTGAGCTAC C-3′; Proximal B, 5′-ACATCCTCACACCACCTGATACTC-3′ and 5′-GAGGCAATGATATCTGTCAGCC-3′; Proximal C, 5′CCCGAAGAATTCCAGCATC-3′ and 5′-CTTTTGCTT C ATCGACAGGG-3′; Proximal D, 5′-GAGTCCTACTCCTG TGCTTGTCTT-3′ and 5′-AGTGTGTGCACATTGTAGGGA G-3′; Proximal E, 5′-GTAAGTTTAGGAAGCAGGGGTCT C-3′ and 5′-GAGGAGGAGACTGCAAGGATAG; Proximal F, 5′-CCTAGCATCGATCTGAACCTATCC-3′ and 5′-GCT GTCACATAACGGGAGTCTAC-3′; and Proximal G, 5′-CC CAGTCTATGAACCTATGGACAG-3′ and 5′-AGGAGTCA GGTCTGTGAGAGATG-3′. Primer sequences for DNA probes distal (telomeric) to *PLP1* include: Distal A, 5′-GAA TGTTGTCAGGTGACCTAGGATT-3′ and 5′-GCAGAGAT GAATTAGGCATGA-3′; Distal B, 5′-ACTGGTAAGGGCT ACTCAACTCAC-3′ and 5′-GAGGTAGTTGGGACTATGT GTGAC-3′; and Distal D, 5′-GTTTGGACCGTGTATTCT CCTC-3′ and 5′-GTCTCTGCTCAAGTTGGGAGTAGT-3′. We amplified these DNA probes by PCR from BAC clone templates prepared by standard alkaline lysis followed by phenol/chloroform extraction, and subsequently isolated the probe DNA by gel extraction (Qiagen).

Southern hybridization

Following the separation of PMD patient and control DNA by PFGE, we transferred DNA to positively charged Sure Blot® Nylon Membranes (Intergen Company) by standard methods for 2 days. We labeled ~200–250 ng of probe DNA with ^{32}P-dCTP (MP Biomedicals) by random priming for at least 2 h at 37°C (Roche). We pre-hybridized membranes with salmon sperm DNA (Sigma) for 4 h and hybridized overnight at 65°C with labeled probes pre-associated with human placental DNA for 1.5–2 h. Subsequently, we analyzed hybridized blots by autoradiography for the presence of bands of expected size and also for bands of varying size, representing recombination-specific junction fragments. We stripped and rehybridized blots with different probes as necessary.

Interphase and metaphase fluorescence *in-situ* hybridization

We harvested cultured lymphoblastoid patient and control cells after Colcemid (Sigma) treatment by standard methods, and dropped them onto glass slides. G-banding was performed by standard methods on all patients with larger duplications except for BAB1327, including BAB2389, 2390, 2396 and 2425. We based our selection of clones to be used as FISH probes for orientation analysis on their presumed full-duplication status determined by custom array CGH described herein. For interphase FISH, we selected BAC clones RP11-1144F22 and RP11-34P3 as FISH probes for duplication orientation analysis of patients BAB1482, 1597, 1334, 1705 and 1707; clones RP11-1123D8 and RP11-462K21 for analysis of patients BAB1261, 1282, 1275 and 1290; clones RP11-1123D8 and RP11-34P3 for analysis of patients BAB1301 and 1305; clones RP11-1123D8 and RP11-454M22 for analysis of patient BAB1420. For metaphase FISH analysis of larger duplications, we selected clones RP11-1001M23 and RP11-462K21 for analysis of patients BAB2389 and 2390; clones CTD-2270O5 and RP11-393D6 for analysis of patient BAB2396; clones RP11-1001M23 and RP11-393D6 for analysis of patient BAB2425. If available, we analyzed the carrier mothers' cells to provide visualization of the signal pattern on the normal X chromosome as a comparison to the duplicated X chromosome.

Each probe pair above has ~51 kb, 323 kb, 314 kb, 694 kb, 3 Mb, 4.5 Mb, and 5 Mb of genomic sequence between them, respectively. We could not test patients BAB1258, 1263 and 1264 for duplication orientation because the furthest duplicated clones, RP11-1123D8 and RP11-34P3, overlap by 84 kb. Orientation analysis was also not done for patient BAB1327. We isolated BAC clone DNA by standard alkaline lysis followed by phenol/chloroform extraction. We labeled

DNA from clones for which pairs have intervening sequence by nick translation either indirectly with digoxigenin (Roche) or biotin (Invitrogen), or directly with SpectrumRed™ or SpectrumGreen™ dUTP (Vysis Inc.). We hybridized probes to interphase and metaphase nuclei on glass slides, counterstained with DAPI (Sigma) in Vectashield (Vector Laboratories Inc.), and visualized the nuclei and metaphase chromosomes by fluorescent microscopy. The order of red and green signals observed, namely red-green-red-green versus red-green-green-red, is indicative of either a direct or inverted duplication, respectively, having occurred in the patient as previously described (48).

Real-time quantitative PCR

As previously described, we performed multiplex real-time quantitative PCR Taqman assays (Applied Biosystems) using a custom probe and primer set designed to ascertain the copy number of a unique region between LCR–PMDA and B (FAM) (29). Assays designed to test the *EIF1AX* gene (FAM) and the RNaseP RNA component *RPPH1* (VIC) were used as X chromosome and loading controls, respectively (Applied Biosystems). Using the following reaction conditions: 95°C for 10 min, followed by 40 cycles of 95°C for 15 s, 60°C for 1 min, we amplified in triplicate 10 ng of genomic DNA. We determined DNA copy number as $2^{-(ddCt)}$ for patients versus a male control.

ACKNOWLEDGEMENTS

We thank the patients and families for their participation in this study, and Sou Saukam for performing G-banding analysis. This work was supported in part by grants from the National Institute of Neurological Disorders and Stroke, NIH (R01 NS27042, J.R.L.), the National Institute for Child Health and Development, NIH (P01 HD38420, J.R.L.), the Baylor College of Medicine Mental Retardation Research Center (HD 2406407), Research Grant for Nervous and Mental Disorders from the Ministry of Health, Labor and Welfare, Japan (16B-1, K.I.), and Health and Labor Science Research Grant, Japan (H18-Kokoro-Ippan-015, K.I.).

Conflict of Interest statement. The authors have no conflicts of interest to declare.

REFERENCES

1. Lupski, J.R. (1998) Genomic disorders: structural features of the genome can lead to DNA rearrangements and human disease traits. *Trends Genet.*, **14**, 417–422.
2. Stankiewicz, P. and Lupski, J.R. (2002) Genome architecture, rearrangements and genomic disorders. *Trends Genet.*, **18**, 74–82.
3. Lupski, J.R. and Stankiewicz, P. (2005) Genomic disorders: molecular mechanisms for rearrangements and conveyed phenotypes. *PLoS Genet.*, **1**, 627–633.
4. Inoue, K., Dewar, K., Katsanis, N., Reiter, L.T., Lander, E.S., Devon, K.L., Wyman, D.W., Lupski, J.R. and Birren, B. (2001) The 1.4-Mb CMT1A duplication/HNPP deletion genomic region reveals unique genome architectural features and provides insights into the recent evolution of new genes. *Genome Res.*, **11**, 1018–1033.
5. Lupski, J.R. (1998) Charcot-Marie-Tooth disease: lessons in genetic mechanisms. *Mol. Med.*, **4**, 3–11.
6. Chen, K.-S., Manian, P., Koeuth, T., Potocki, L., Zhao, Q., Chinault, A.C., Lee, C.C. and Lupski, J.R. (1997) Homologous recombination of a flanking repeat gene cluster is a mechanism for a common contiguous gene deletion syndrome. *Nat. Genet.*, **17**, 154–163.
7. Chen, K.-S., Potocki, L. and Lupski, J.R. (1996) The Smith-Magenis syndrome [del(17)p11.2]: clinical review and molecular advances. *Ment. Retard. Dev. Disabil. Res. Rev.*, **2**, 122–129.
8. Peoples, R., Franke, Y., Wang, Y.-K., Pérez-Jurado, L., Paperna, T., Cisco, M. and Francke, U. (2000) A physical map, including a BAC/PAC clone contig, of the Williams-Beuren syndrome—deletion region at 7q11.23. *Am. J. Hum. Genet.*, **66**, 47–68.
9. Morris, C.A., Demsey, S.A., Leonard, C.O., Dilts, C. and Blackburn, B.L. (1988) Natural history of Williams syndrome: physical characteristics. *J. Pediatr.*, **113**, 318–326.
10. Inoue, K. and Lupski, J.R. (2002) Molecular mechanisms for genomic disorders. *Annu. Rev. Genom. Hum. Genet.*, **3**, 199–242.
11. Garbern, J., Cambi, F., Shy, M. and Kamholz, J. (1999) The molecular pathogenesis of Pelizaeus-Merzbacher disease. *Arch. Neurol.*, **56**, 1210–1214.
12. Hodes, M.E., Pratt, V.M. and Dlouhy, S.R. (1993) Genetics of Pelizaeus-Merzbacher disease. *Dev. Neurosci.*, **15**, 383–394.
13. Inoue, K. (2005) *PLP1*-related inherited dysmyelinating disorders: Pelizaeus-Merzbacher disease and spastic paraplegia type 2. *Neurogenetics*, **6**, 1–16.
14. Inoue, K., Osaka, H., Imaizumi, K., Nezu, A., Takanashi, J.-i., Arii, J., Murayama, K., Ono, J., Kikawa, Y., Mito, T. *et al.* (1999) Proteolipid protein gene duplications causing Pelizaeus-Merzbacher disease: molecular mechanism and phenotypic manifestations. *Ann. Neurol.*, **45**, 624–632.
15. Sistermans, E.A., de Coo, R.F.M., De Wijs, I.J. and Van Oost, B.A. (1998) Duplication of the proteolipid protein gene is the major cause of Pelizaeus-Merzbacher disease. *Neurology*, **50**, 1749–1754.
16. Mattei, M.G., Alliel, P.M., Dautigny, A., Passage, E., Pham-Dinh, D., Mattei, J.F. and Jollès, P. (1986) The gene encoding for the major brain proteolipid (PLP) maps on the q-22 band of the human X chromosome. *Hum. Genet.*, **72**, 352–353.
17. Willard, H.F. and Riordan, J.R. (1985) Assignment of the gene for myelin proteolipid protein to the X chromosome: implications for X-linked myelin disorders. *Science*, **230**, 940–942.
18. Inoue, K., Osaka, H., Thurston, V.C., Clarke, J.T.R., Yoneyama, A., Rosenbarker, L., Bird, T.D., Hodes, M.E., Shaffer, L.G. and Lupski, J.R. (2002) Genomic rearrangements resulting in *PLP1* deletion occur by non-homologous end joining and cause different dysmyelinating phenotypes in males and females. *Am. J. Hum. Genet.*, **71**, 838–853.
19. Woodward, K.J., Cundall, M., Sperle, K., Sistermans, E.A., Ross, M., Howell, G., Gribble, S.M., Burford, D.C., Carter, N.P., Hobson, D.L. *et al.* (2005) Heterogeneous duplications in patients with Pelizaeus-Merzbacher disease suggest a mechanism of coupled homologous and nonhomologous recombination. *Am. J. Hum. Genet.*, **77**, 966–987.
20. Hudson, L.D. (2001) Pelizaeus-Merzbacher disease and the allelic disorder X-linked spastic paraplegia type 2. In Scriver, C.R., Beaudet, A.L., Sly, W.S. and Valle, D. (eds), *The Metabolic and Molecular Basis of Inherited Diseases*, 8th edn. McGraw-Hill, New York, Vol. IV, pp. 5789–5798.
21. Woodward, K., Kendall, E., Vetrie, D. and Malcolm, S. (1998) Pelizaeus-Merzbacher disease: identification of Xq22 proteolipid-protein duplications and characterization of breakpoints by interphase FISH. *Am. J. Hum. Genet.*, **63**, 207–217.
22. Shaw, C.J. and Lupski, J.R. (2004) Implications of human genome architecture for rearrangement-based disorders: the genomic basis of disease. *Hum. Mol. Genet.*, **13**, R57–R64.
23. Stankiewicz, P., Shaw, C.J., Dapper, J.D., Wakui, K., Shaffer, L.G., Withers, M., Elizondo, L., Park, S.-S. and Lupski, J.R. (2003) Genome architecture catalyzes non-recurrent chromosomal rearrangements. *Am. J. Hum. Genet.*, **72**, 1101–1116.
24. Reiter, L.T., Murakami, T., Koeuth, T., Gibbs, R.A. and Lupski, J.R. (1997) The human *COX10* gene is disrupted during homologous recombination between the 24 kb proximal and distal CMT1A-REPs. *Hum. Mol. Genet.*, **6**, 1595–1603.
25. Park, S.-S., Stankiewicz, P., Bi, W., Shaw, C., Lehoczky, J., Dewar, K., Birren, B. and Lupski, J.R. (2002) Structure and evolution of the Smith-Magenis syndrome repeat gene clusters, SMS-REPs. *Genome Res.*, **12**, 729–738.

26. Stankiewicz, P., Shaw, C.J., Withers, M., Inoue, K. and Lupski, J.R. (2004) Serial segmental duplications during primate evolution result in complex human genome architecture. *Genome Res.*, **14**, 2209–2220.
27. Kurotaki, N., Stankiewicz, P., Wakui, K., Niikawa, N. and Lupski, J.R. (2005) Sotos syndrome common deletion is mediated by directly oriented subunits within inverted Sos-REP low-copy repeats. *Hum. Mol. Genet.*, **14**, 535–542.
28. Visser, R., Shimokawa, O., Harada, N., Kinoshita, A., Ohta, T., Niikawa, N. and Matsumoto, N. (2005) Identification of a 3.0-kb major recombination hotspot in patients with Sotos syndrome who carry a common 1.9-Mb microdeletion. *Am. J. Hum. Genet.*, **76**, 52–67.
29. Lee, J.A., Madrid, R.E., Sperle, K., Ritterson, C.M., Hobson, G.M., Garbern, J., Lupski, J.R. and Inoue, K. (2006) Spastic paraplegia type 2 associated with axonal neuropathy and apparent *PLP1* position effect. *Ann. Neurol.*, **59**, 398–403.
30. Hodes, M.E., Woodward, K., Spinner, N.B., Emanuel, B.S., Enrico-Simon, A., Kamholz, J., Stambolian, D., Zackai, E.H., Pratt, V.M., Thomas, I.T. *et al.* (2000) Additional copies of the proteolipid protein gene causing Pelizaeus-Merzbacher disease arise by separate integration into the X chromosome. *Am. J. Hum. Genet.*, **67**, 14–22.
31. Iwaki, A., Kondo, J., Ototsuji, M., Kurosawa, K. and Fukumaki, Y. (2003) Characterization of the breakpoints of PLP1 duplication in three cases of Pelizaeus-Merzbacher disease. *Am. J. Hum. Genet.*, **73** (suppl.), 549.
32. Shaw, C.J. and Lupski, J.R. (2005) Non-recurrent 17p11.2 deletions are generated by homologous and non-homologous mechanisms. *Hum. Genet.*, **116**, 1–7.
33. Mimault, C., Giraud, G., Courtois, V., Cailloux, F., Boire, J.Y., Dastugue, B. and Boespflug-Tanguy, O. (1999) Proteolipoprotein gene analysis in 82 patients with sporadic Pelizaeus-Merzbacher Disease: duplications, the major cause of the disease, originate more frequently in male germ cells, but point mutations do not. The Clinical European Network on Brain Dysmyelinating Disease. *Am. J. Hum. Genet.*, **65**, 360–369.
34. Hu, X., Ray, P.N. and Worton, R.G. (1991) Mechanisms of tandem duplication in the Duchenne muscular dystrophy gene include both homologous and nonhomologous intrachromosomal recombination. *EMBO J.*, **10**, 2471–2477.
35. Heath, J.D. and Weinstock, G.M. (1991) Tandem duplications of the *lac* region of the *Escherichia coli* chromosome. *Biochimie*, **73**, 343–352.
36. Woodward, K., Cundall, M., Palmer, R., Surtees, R., Winter, R.M. and Malcolm, S. (2003) Complex chromosomal rearrangement and associated counseling issues in a family with Pelizaeus-Merzbacher disease. *Am. J. Med. Genet.*, **118A**, 15–24.
37. Ida, T., Miharu, N., Hayashitani, M., Shimokawa, O., Harada, N., Samura, O., Kubota, T., Niikawa, N. and Matsumoto, N. (2003) Functional disomy for Xq22-q23 in a girl with complex rearrangements of chromosomes 3 and X. *Am. J. Med. Genet.*, **120A**, 557–561.
38. Wolf, N.I., Sistermans, E.A., Cundall, M., Hobson, G.M., Davis-Williams, A.P., Palmer, R., Stubbs, P., Davies, S., Endziniene, M., Wu, Y. *et al.* (2005) Three or more copies of the proteolipid protein gene *PLP1* cause severe Pelizaeus-Merzbacher disease. *Brain*, **128**, 743–751.
39. Combes, P., Bonnet-Dupeyron, M.-N., Gauthier-Barichard, F., Schiffmann, R., Bertini, E., Rodriguez, D., Armour, J.A.L., Boespflug-Tanguy, O. and Vaurs-Barrière, C. (2006) *PLP1* and *GPM6B* intragenic copy number analysis by MAPH in 262 patients with hypomyelinating leukodystrophies: identification of one partial triplication and two partial deletions of. *PLP1. Neurogenetics*, **7**, 31–37.
40. Eichler, E.E. (1998) Masquerading repeats: paralogous pitfalls of the human genome. *Genome Res.*, **8**, 758–762.
41. Johnson, R.D. and Jasin, M. (2000) Sister chromatid gene conversion is a prominent double-strand break repair pathway in mammalian cells. *EMBO J.*, **19**, 3398–3407.
42. Richardson, C. and Jasin, M. (2000) Coupled homologous and nonhomologous repair of a double-strand break preserves genomic integrity in mammalian cells. *Mol. Cell. Biol.*, **20**, 9068–9075.
43. Tatusova, T.A. and Madden, T.L. (1999) BLAST 2 sequences, a new tool for comparing protein and nucleotide sequences. *FEMS Microbiol. Lett.*, **174**, 247–250.
44. Kent, W.J., Sugnet, C.W., Furey, T.S., Roskin, K.M., Pringle, T.H., Zahler, A.M. and Haussler, D. (2002) The human genome browser at UCSC. *Genome Res.*, **12**, 996–1006.
45. Karolchik, D., Baertsch, R., Diekhans, M., Furey, T.S., Hinrichs, A., Lu, Y.T., Roskin, K.M., Schwartz, M., Sugnet, C.W., Thomas, D.J. *et al.* (2003) The UCSC Genome Browser Database. *Nucleic Acids Res.*, **31**, 51–54.
46. Inoue, K., Kanai, M., Tanabe, Y., Kubota, T., Kashork, C.D., Wakui, K., Fukushima, Y., Lupski, J.R. and Shaffer, L.G. (2001) Prenatal interphase FISH diagnosis of *PLP1* duplication associated with Pelizaeus-Merzbacher disease. *Prenat. Diagn.*, **21**, 1133–1136.
47. Lee, J.A., Cheung, S.W., Ward, P.A., Inoue, K. and Lupski, J.R. (2005) Prenatal diagnosis of *PLP1* copy number by array comparative genomic hybridization. *Prenat. Diagn.*, **25**, 1188–1191.
48. Potocki, L., Chen, K.-S., Park, S.-S., Osterholm, D.E., Withers, M.A., Kimonis, V., Summers, A.M., Meschino, W.S., Anyane-Yeboa, K., Kashork, C.D. *et al.* (2000) Molecular mechanism for duplication 17p11.2—the homologous recombination reciprocal of the Smith-Magenis microdeletion. *Nat. Genet.*, **24**, 84–87.

Spanish Fondo de Investigación Sanitaria (FIS-04-0009, E. L.-G., J. M.), and Networks for Mitochondrial Disorders and Ataxias (G03-011/G03-056, M.P., A.O., E. L.-G., A.N., A.S., M.D. H., M.A.V., P.B., J.M., R.A.).

References

1. Zeviani M, Moraes CT, DiMauro S, et al. Deletions of mitochondrial DNA in Kearns-Sayre syndrome. Neurology 1988;38:1339–1346.
2. Allen J, DiMauro S, Coulter D, et al. Kearns-Sayre syndrome with reduced plasma and cerebrospinal fluid folate. Ann Neurol 1983;13,6:679–681.
3. Dougados M, Zittoun J, Laplane D, Castaigne P. Folate metabolism disorder in Kearns-Sayre syndrome. Ann Neurol 1983;13:679–682.
4. Artuch R, Vilaseca MA, Farré C, Ramón F. Determination of lactate, pyruvate, B-hydroxybutyrate and acetoacetate with a centrifugal analyser. Eur J Clin Chem Clin Biochem 1995;33:529–533.
5. Moyano D, Vilaseca MA, Artuch R, Lambruschini N. Plasma amino acids in anorexia nervosa. Eur J Clin Nutr 1998;52:684–689.
6. Belz S, Frickel C, Wolfrom C, et al. High-performance liquid chromatographic determination of methotrexate, 7-hydroxymethotrexate, 5-methyltetrahydrofolic acid and folinic acid in serum and cerebrospinal fluid. J Chromatogr B Biomed Appl 1994;661:109–118.
7. Ormazabal A, García-Cazorla A, Fernández Y, et al. HPLC with electrochemical and fluorescence detection procedures for the diagnosis of inborn errors of biogenic amines and pterins. J Neurosci Methods 2005;142:153–158.
8. Rustin P, Chretien D, Bourgeron T, et al. Biochemical and molecular investigations in respiratory chain deficiencies. Clin Chim Acta 1994;228:35–51.
9. Fischer JC, Ruitenbeek W, Berden Já, et al. Differential investigation of the capacity of succinate oxidation in human skeletal muscle. Clin Chim Acta 1985;153:23–36.
10. Lowry OH, Rosenbrough NJ, Farr AL, Randall RJ. Protein measurement with the folin phenol reagent. J Biol Chem 1951;193:265–275.
11. Barragan-Campos HM, Vallee JN, Lo D, Barrera-Ramirez CF, et al. Brain magnetic resonance imaging findings in patients with mitochondrial cytopathies.Arch Neurol 2005;62:737–742.
12. Ramaekers VT, Blau N. Cerebral folate deficiency. Dev Med Child Neurol 2004;46:843–851.
13. Tanji K, Schon EA, DiMauro S, Bonilla E. Kearns-Sayre syndrome: oncocytic transformation of choroids plexus epithelium. J Neurol Sci 2000;178:29–36.
14. Surtees R, Leonard J, Austin S. Association of demyelination with deficiency of cerebrosinal-fluid S-adenosylmethionine in inborn errors of methyl-transfer pathway. Lancet 1991;338:1550–1554.
15. Ramaekers VT, Rothenberg SP, Sequeira JM, et al. Autoantibodies to folate receptors in the cerebral folate deficiency syndrome. N Engl J Med 2005;352:1985–1991.
16. Surtees R, Heales S, Bowron A. Association of cerebrospinal fluid deficiency of 5-methyltetrahydrofolate, but not S-adenosylmethionine, with reduced concentrations of the acid metabolites of 5-hydroxytryptamine and dopamine. Clin Sci 1994;86:697–702.
17. Hansen FJ, Blau N. Cerebral folate deficiency: life-changing supplementation with folinic acid. Mol Genet Metab 2005;84:371–373.
18. Crott JW, Choi SW, Branda RF, Mason JB. Accumulation of mitochondrial DNA deletions is age, tissue and folate-dependent in rats. Mut Res 2005;570:63–70.

Spastic Paraplegia Type 2 Associated with Axonal Neuropathy and Apparent *PLP1* Position Effect

Jennifer A. Lee, BS,[1] Ricardo E. Madrid, MD,[2] Karen Sperle, MS,[3] Carolyn M. Ritterson, BS,[4] Grace M. Hobson, PhD,[5,5] James Garbern, MD, PhD,[6] James R. Lupski, MD, PhD,[1,7,8] and Ken Inoue, MD, PhD[1,9]

Objective: **To report an association between spastic paraplegia type 2 with axonal peripheral neuropathy and apparent proteolipid protein gene (*PLP1*) silencing in a family.** ***Methods:*** **Pulsed-field gel electrophoresis, custom array comparative genomic hybridization, and semi-quantitative multiplex polymerase chain reaction analyses were used to examine the *PLP1* genomic region.** ***Results:*** **Electrodiagnostic studies and a sural nerve biopsy showed features of a dystrophic axonal neuropathy. Molecular studies identified a small duplication downstream of *PLP1*.** ***Interpretation:*** **We propose the duplication to result in *PLP1* gene silencing by virtue of a position effect. Our observations suggest that genomic rearrangements that do not include *PLP1* coding sequences should be considered as yet another potential mutational mechanism underlying *PLP1*-related dysmyelinating disorders.**

Ann Neurol 2006;59:398–403

Pelizaeus–Merzbacher disease (PMD) and spastic paraplegia type 2 (SPG2) are clinically distinct allelic disorders, yet represent a wide spectrum of central ner-

From the [1]Department of Molecular and Human Genetics, Baylor College of Medicine, Houston, TX; [2]New York State Institute for Basic Research in Developmental Disabilities, George A. Jervis Clinic, Staten Island, NY; [3]Nemours Biomedical Research, Alfred I. duPont Hospital for Children, Nemours Children's Clinic, Wilmington, DE; [4]Department of Biology, Boston University, Boston, MA; [5]Department of Pediatrics, Jefferson Medical College, Philadelphia, PA; [6]Department of Neurology and Center of Molecular Medicine and Genetics, Wayne State University School of Medicine, Detroit, MI; [7]Department of Pediatrics, Baylor College of Medicine and [8]Texas Children's Hospital, Houston, TX; and [9]Department of Mental Retardation and Birth Defect Research, National Institute of Neuroscience, National Center of Neurology and Psychiatry, Tokyo, Japan.

Received Mar 23, 2005, and in revised form Aug 24 and Sep 28. Accepted for publication Sep 29, 2005.

Published online Dec 22, 2005, in Wiley InterScience (www.interscience.wiley.com). DOI: 10.1002/ana.20732

Address correspondence to Dr Inoue, Department of Mental Retardation and Birth Defect Research National, Institute of Neurology National Center of Neurology and Psychiatry (NCNP), 4-1-1 Ogawahigashi, Kodaira, Tokyo 187-8502.
E-mail: kinoue@ncnp.go.jp

Table. Sensory and Motor Nerve Conduction Study Measurements

	Median Nerve			Ulnar Nerve			Sural Nerve			Superficial Peroneal Nerve		
	On. Lat. (msec)	Pk. Lat. (msec)	Amp. (μV)	On. Lat. (msec)	Pk. Lat. (msec)	Amp. (μV)	On. Lat. (msec)	Pk. Lat. (msec)	Amp. (μV)	On. Lat. (msec)	Pk. Lat. (msec)	Amp. (μV)
Patient	3.5	4.2	7.6	2.7	3.5	18	NR	0	0	NR	0	0
Reference	<2.5	<3.6	>10	<2.1	<3.7	>15	<2.8	<3.4	>5.0	<2.9	<3.0	>20

	Median Nerve			Ulnar Nerve			Tibial Nerve		
	AMP	DL (msec)	CV (m/sec)	AMP	DL (msec)	CV (m/sec)	AMP	DL (msec)	CV (m/sec)
Patient	7.9	3.9	62	4.4	3.3	59	1.8	5.6	40.2
Reference	>6.0	<3.8	>54	>10.0	<3.0	>52	>8.0	<4.8	>40

Sensory nerve conduction measurements are shown in the first section, and motor nerve conduction measurements are shown in the second section for the patient versus reference values.

On. Lat. = onset latency; Pk. Lat. = peak latency; Amp. = amplitude; AMP = compound muscle action potential; DL = distal latency; CV = conduction velocity; NR = no response.

vous system (CNS) dysmyelination associated with mutations in the Xq22.2 proteolipid protein gene (*PLP1*). Approximately 80 to 90% of PMD/SPG2 patients have *PLP1* mutations, including duplication, deletion, and point mutations in exons or splice junctions.[1–3] Patients with *PLP1* null mutations show PMD/SPG2 at the mild end of the disease spectrum[4] and peripheral neuropathy.[5,6]

The remaining 10 to 20% of patients show no apparent *PLP1* abnormalities; either these are caused by genetic heterogeneity,[7–9] or there may be other types of *PLP1* mutations that remain to be discovered. We report a patient with a phenotype consisting of a unique combination of SPG2 and axonal neuropathy. After exclusion of all types of known *PLP1* coding and rearrangement mutations, we identified a small duplication downstream of *PLP1*. We hypothesize that this duplication is silencing *PLP1* expression, resulting in a phenotype similar to that caused by *PLP1* null mutations.

Case Report

A 28-year-old Jamaican man (BAB1612) presented with a history of frequent falls, awkward gait, dense dysarthria, swallowing difficulties due to a right congenital branchial sinus, pectus carinatum, and moderate mental retardation since infancy. No family history of neurological diseases was noted. His independent but steppage gait worsened from age 21 years. Currently, he uses a wheelchair but can ambulate with assistance, shows generalized muscle atrophy and weakness, claw hands, bilateral pes cavus, and hammer toes. A spastic paraplegia with absent ankle jerks was found. With his arms outstretched, a dystonic posture of both hands is evident. Metachromatic leukodystrophy and adrenomyeloneuropathy were excluded by biochemical testing.

Nerve conduction studies showed normal velocities but reduced amplitudes (Table). An electromyogram showed length-dependent denervation, as it was found in distal, not proximal, muscles. Axial fluid-attenuated inversion recovery (FLAIR) brain magnetic resonance imaging (MRI) showed mild hyperintensity in the posterior periventricular white matter (Fig 1A). The C2 level spinal cord cross-sectional area on T1-weighted MRI was 55mm^2 (reference, 93.9 ± 11.4mm^2),[10] signifying atrophy, which was also seen in the cerebellum and brainstem.

Results

Sural Nerve Biopsy

A sural nerve biopsy specimen was processed for light microscopy, teased fibers, and electron microscopy using standard techniques. The transverse fascicular area and diameter distribution of myelinated and unmyelinated fibers were determined. Myelinated fiber density was reduced at 3,666/mm^2 (age-matched control, 7,709/mm^2; see Fig 1B). The numbers of large and small fibers were decreased, whereas unmyelinated axon density was within reference limits. Myelin chambers and clusters of small myelinated fibers denoted the presence of axonal degeneration and regeneration (see Fig 1C). Thus, the measured density may be an underestimate of the loss of the myelinated fibers originally present. Approximately 24.7% of the teased fibers showed axonal degeneration or regeneration (reference range up to 7.6%).[11] Abnormal segmental demyelination or remyelination was not observed. By electron microscoscopy, axonal accumulation of normal and giant mitochondria in unmyelinated and myelinated fibers was frequently found (see Fig 1D, E). Approximately 24% of myelinated fibers had at least 10

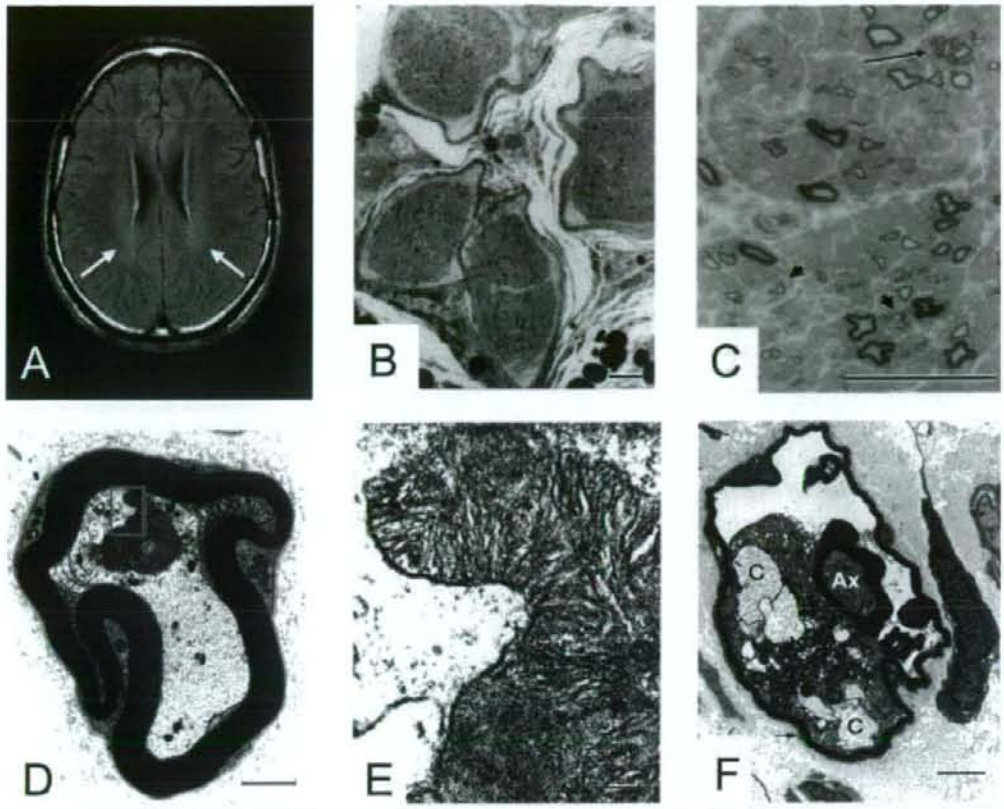

Fig 1. Brain magnetic resonance imaging (MRI) (A) and light (B, C) and electron (D– F) microscopy of sural nerve. (A) An axial fluid-attenuated inversion recovery (FLAIR) image showing areas of mild hyperintensity in the periventricular white matter in the patient (arrows). *(B) Sural nerve, low-power view showing reduced density of myelinated fibers. Toluidine blue stain, 1μm thick plastic section. Bar = 100μm. (C) High-power view of the upper left fascicle in (B). Note cluster of eight regenerating fibers* (long arrow). *Single regenerating fibers showing redundant myelin loops are also seen* (short arrows). *Bar = 50μm. (D) Hypertrophic mitochondrion within an otherwise normal axoplasm of this myelinated fiber. The area of the rectangle is shown at higher magnification in (E). Bar = 1μm. (E) Increased number of cristae with their membranes in various stages of apposition. Bar = 100nm. (F) A serially cut nerve fiber with focal axonal dystrophy and focally distended myelin sheath is seen. Note the distinctive tubulovesicular elements* (arrow) *that surround the lower axonal cleft,* C. *The axon is indicated with* Ax. *A cluster of abnormal mitochondria occupies most of the axoplasm wedged between the two clefts. Bar = 2μm.*

normal or at least one giant mitochondrion in their axons, the latter showing membrane proliferation apposed in whorls. Numerous abnormal mitochondria were found in focal axonal swellings with secondary thinning of the fiber's myelin sheath. The axon of one such fiber, serially cut over 50μm, showed membrane-bound clefts and tubulovesicular profiles (see Fig 1F); these axonal spheroids were found in 1.5% of myelinated fibers. We investigated whether *PLP1* expression is decreased in the patient's nerve tissue using quantitative reverse transcription polymerase chain reaction (RT-PCR); the results were inconclusive in this pathological specimen.

Absence of PLP1 Rearrangement or Coding Region Mutations

Fluorescence in situ hybridization (FISH) of interphase nuclei suggested that *PLP1* is present in normal copy number (data not shown). Southern analysis of *PLP1* and its promoter region, and PCR amplification of overlapping amplicons throughout the gene and promoter region, indicated no intragenic disruption (data not shown). DNA sequencing analysis of *PLP1* coding exons, splice junctions, and promoter showed no alterations. Additionally, no mutations were identified in the gap junction protein B1, myelin protein zero, and neurofilament light chain genes (data not shown).

Altered Dosage for Genomic Region Downstream of PLP1

Semiquantitative PCR analysis was performed on the DNA from the patient and controls using a series of primer pairs multiplexed with a control primer from a region on Xp. Amplicon intensities were analyzed to determine DNA dosage of *PLP1* and the surrounding genomic region. No increased dosage was observed for the *PLP1* gene. However, surprisingly, there was increased dosage of a 100 to 150kb genomic region 135 to 185kb downstream of *PLP1* (Fig 2A, B).

Genomic Duplication Rearrangement Downstream of PLP1

Using pulsed-field gel electrophoresis (PFGE) to separate high molecular weight genomic DNA and Southern analysis of this genomic region, we observed junction fragments, revealing a genomic rearrangement in both the patient and his mother (Fig 2C, D). Restriction mapping suggested a duplication of less than 150kb approximately 136kb downstream of *PLP1*, consistent with semiquantitative PCR data. Duplication polymorphism was excluded by quantitative real-time PCR, array comparative genomic hybridization (aCGH), or semiquantiative PCR dosage testing in 367 control individuals. Interestingly, four Caucasian controls showed evidence for copy number variation in the region of low-copy repeat (LCR) PMDs[6] but did not have the duplication reported in the proband (data not shown).

Comparative Genomic Hybridization and Fluorescent In Situ Hybridization Confirm Downstream Duplication

Custom aCGH[12] encompassing an approximately 10Mb region including *PLP1* was utilized to assay for DNA dosage. aCGH analysis showed a gain in signal intensity for a single bacterial artificial chromosome (BAC) clone RP11-462K21, indicating duplication of this genomic region in the patient and mother (see Fig 2E, F). Interphase FISH analysis using a RP11-462K21 probe confirmed the duplication in the patient (see Fig 2G) and mother (data not shown). X-inactivation status of the carrier mother was assayed by screening the proportion of duplicated X chromosomes versus the proportion of normal X chromosomes that appear as Barr bodies (59:41) and showed an essentially random X-inactivation pattern. No other chromosomal abnormalities were found.

Discussion

We identified a family with SPG2 wherein the phenotype is likely caused by a downstream duplication potentially affecting *PLP1* expression; we excluded duplication, deletion, and point mutation of the *PLP1* gene. We propose position effect as the fourth type of *PLP1* mutation causing SPG2, and possibly PMD as well. Such position effects may account for some of the SPG2/PMD patients for which no apparent abnormalities in *PLP1* have been found. Because the clinical phenotype observed, particularly the associated peripheral neuropathy, is similar to that of a null mutation causing SPG2 or the mildest form of PMD, we speculate that reduced *PLP1* expression is probably the underlying mechanism.

The axonal spheroids found in the nerve biopsy contained abnormal mitochondria and distinctive tubulovesicular profiles. These abnormalities are demonstrated here for the first time in the peripheral nervous system (PNS) of an SPG2 patient. It is unclear why axonopathy with such dystrophic changes dominates in our case rather than demyelinating neuropathy as observed in previously reported null *PLP1* cases.[5,6] As in the central axons of *Plp1* knockout or low-level *Plp1* expressing transgenic mice,[13,14] profound CNS axonal abnormalities have been demonstrated in PMD patients by magnetic resonance spectroscopy studies,[2,15] suggesting disruption of trophic myelin–axon interactions. Similarly, decreased *PLP1* expression in Schwann cells may affect interacting axons, causing peripheral axonal neuropathy, if *PLP1* is necessary for proper myelin–axon interaction in a normal PNS.

The only genetic abnormality detected was a genomic duplication of less than 150kb and located approximately 136kb downstream of *PLP1*. The duplication lies within RP11-462K21, a BAC containing low-copy repeats LCR-PMDA and B. These LCRs have been found at or near many *PLP1* duplication[21] (and our unpublished data) and deletion[6] distal breakpoints and have been implicated in stimulating rearrangement in this region of the genome.

Examples of human diseases caused by disruption of long-range control of gene expression were recently discussed.[16] Also, a patient with an inv(X)(p22.3;q22) and mild PMD symptoms possibly caused by a position effect with a chromosomal breakage 70kb upstream of *PLP1* was reported.[17] Considering that report and the duplication in our patient, transcriptional regulatory elements of *PLP1* are likely present within an extended genomic interval. Decreased expression may result from silencing regulatory element duplication or enhancer disruption. Computational analysis of the duplicated region showed genes *H2BFWT* (testis-specific histone 2B gene) and *MGC39900* (predicted thymosin β4 gene, actin-binding), histone pseudogenes and other pseudogenes, and potential regulatory elements including CpG islands, predicted promoters, and predicted/conserved transcription factor binding sites, in addition to high evolutionary sequence conservation and regions of three-way (human, mouse, and rat) regulatory potential (Ensembl; NIX; UCSC Genome Browser). Increased dosage of the included genes is likely not causative for either CNS or PNS pheno-

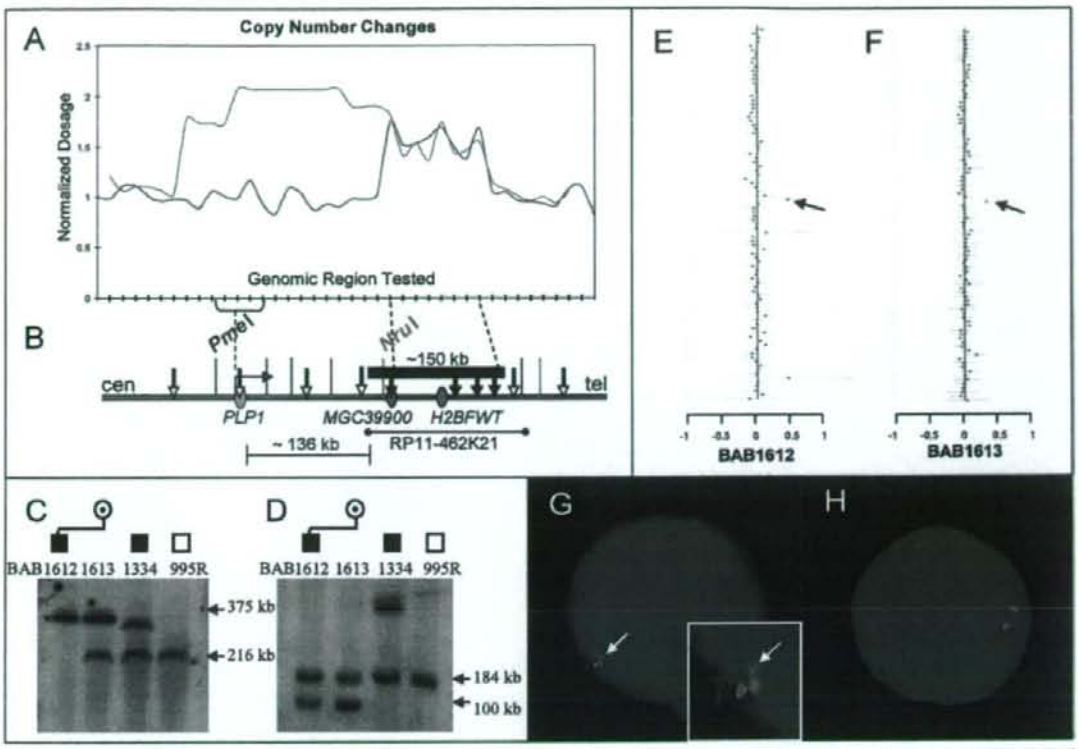

Fig 2. Genetic analyses. (Top left) Graphical representation of normalized dosage tested by semiquantitative polymerase chain reaction (PCR), aligned (dotted lines) *with the genomic region tested. (A) Analysis of BAB1612 shows a duplication downstream of* PLP1 (dark blue line), *and a* PLP1 *duplication patient is shown* (green line) *as a positive control. Tick marks on the* x *axis represent the primer pairs within P1 artificial chromosome (PAC) and cosmid clones tested (see on-line supplement). (B)* PLP1, MGC39900, *and* H2BFWT *genes are shown, in addition to restriction enzyme recognition sites for* PmeI *(purple) and* NruI *(pink). Open-headed arrows indicate representative regions negative for, and closed-headed arrows indicate representative regions positive for, duplication by PCR. Black horizontal bar represents region shown to be duplicated by PCR and pulsed-field gel electrophoresis (PFGE) data combined. Approximate genomic distances are shown, as well as alignment with bacterial artificial chromosome (BAC) clone RP11-462K21. (bottom left) PFGE analysis to assay for genomic rearrangement in Patient BAB1612 and his mother BAB1613, with an unrelated* PLP1 *duplication patient (BAB1334), whose distal breakpoint is in the vicinity of low-copy repeats LCR-PMDA and B, and a negative control (BAB995R) for comparison. The hybridization probe used was designed just proximal to LCR-PMDA and B. (C)* PmeI*-digested DNA shows a junction fragment of 375kb in the patient and carrier mother, in addition to a 216kb band in the mother from her normal X chromosome. The expected band size in a normal individual is 216kb, as shown for BAB995R. These junction fragments were not observed in 10 control individuals (data not shown). (D)* NruI*-digested DNA shows a junction fragment of 100kb in the patient and carrier mother, in addition to a 184kb band in the mother from her normal X chromosome. Expected band size is 184kb. These junction fragments were not observed in five control individuals (data not shown). (top right) Normalized array comparative genomic hybridization (aCGH) data from an array including 68 BAC and PAC large-insert clones for (E) Patient BAB1612 and (F) his mother BAB1613, respectively. A single BAC clone, RP11-462K21* (arrow), *is duplicated in both individuals. (bottom right) Interphase FISH analysis confirms duplication detected by aCGH and PCR. BAC clone RP11-462K21 was labeled (by direct labeling) in red, whereas PAC RP1-39B6 was labeled in green as an X chromosome control. (G) Patient BAB1612 shows a duplicated red signal* (arrow). *(H) Fluorescence in situ hybridization analysis of a male control.*

types, because *H2BFWT* is proposed to have a specialized role in spermatogenesis,[18] and *MGC39900*, although expressed in brain, is not expressed in peripheral nerve tissue (NCBI UniGene). Furthermore, *PLP1* genomic duplications spanning this region do not confer further CNS or PNS manifestations of the PMD phenotype than that caused by smaller duplication not spanning this region[19] or intragenic *PLP1* point mutations.

Our patient exhibited a phenotype at the mild end

of the PMD/SPG2 spectrum with subtle hyperintensity in white matter only detectable by FLAIR MRI (see Fig 1A), a clinical finding that is similar to, but also atypically mild for, that caused by *PLP1* null mutations. Dystrophic axonal neuropathy with minimal demyelination is also a peculiar feature. Interestingly, altered expression of a causative gene by position effect commonly confers a phenotype different from that observed with gene mutations.[16] Thus, silencing by position effect may not result in exactly the same PMD/SPG2 phenotype as by *PLP1* null mutation; instead a partial or incomplete phenotype may arise, similar to that reported for the mild campomelic dysplasia phenotype associated with *SOX9* position effect.[20] We predict that gene regulation by position effect is causative for many more subsets of clinical symptoms associated with human genetic disease than previously anticipated, including but not limited to PMD/SPG2.

The URLs for data presented herein are as follows: Ensembl, http://www.ensembl.org/; NIX, http://www.hgmp.mrc.ac.uk/NIX/; UCSC Genome Browser, http://genome.ucsc.edu/; NCBI UniGene, http://www.ncbi.nlm.nih.gov/entrez/query.fcgi?db = unigene; supplemental information can be viewed at http://www.imgen.bcm.tmc.edu/molgen/lupski/

This study was supported by grants from Muscular Dystrophy Association (K.I., J.R.L.); a grant from Nervous and Mental Disorders from Ministry of Health, Labor and Welfare (16B-1; K.I.); NIH (National Institute for Neurological Disorders and Stroke, R01 NS27042; J.R.L.), National Institute for Child Health and Development, P01 HD38420; J.R.L.); New York State Office of Mental Retardation and Developmental Disabilities (R.E.M.); the Nemours Foundation, the PMD Foundation, the Kylan Hunter Foundation, and NIH National Center for Research Resources (1P20RR020173; G.M.H.).

We thank the patient and his family for their cooperation in this study. We also thank Drs. S. A. Yatsenko and S. W. Cheung for FISH diagnosis, Dr C. A. Shaw for aCGH statistical analysis, Dr G. J. Snipes for helpful advice, Dr P. Stankiewicz for critical review, and Dr H. Takashima for providing control nerve samples.

Some of the results reported here were originally presented at the 53rd annual meeting of the American Academy of Neurology, Philadelphia, PA, 4/01.

References

1. Garbern J, Cambi F, Shy M, Kamholz J. The molecular pathogenesis of Pelizaeus-Merzbacher disease. Arch Neurol 1999;56:1210–1214.
2. Inoue K. *PLP1*-related inherited dysmyelinating disorders: Pelizaeus-Merzbacher disease and spastic paraplegia type 2. Neurogenetics 2005;6:1–16.
3. Inoue K, Osaka H, Imaizumi K, et al. Proteolipid protein gene duplications causing Pelizaeus-Merzbacher disease: molecular mechanism and phenotypic manifestations. Ann Neurol 1999;45:624–632.
4. Cailloux F, Gauthier-Barichard F, Mimault C, et al. Genotype-phenotype correlation in inherited brain myelination defects due to proteolipid protein gene mutations. Eur J Hum Genet 2000;8:837–845.
5. Garbern JY, Cambi F, Tang X-M, et al. Proteolipid protein is necessary in peripheral as well as central myelin. Neuron 1997;19:205–218.
6. Inoue K, Osaka H, Thurston VC, et al. Genomic rearrangements resulting in *PLP1* deletion occur by nonhomologous end joining and cause different dysmyelinating phenotypes in males and females. Am J Hum Genet 2002;71:838–853.
7. Osaka H, Kawanishi C, Inoue K, et al. Pelizaeus-Merzbacher disease: three novel mutations and implication for locus heterogeneity. Ann Neurol 1999;45:59–64.
8. Lazzarini A, Schwarz KO, Jiang S, et al. Pelizaeus-Merzbacher-like disease: exclusion of the proteolipid protein locus and documentation of a new locus on Xq. Neurology 1997;49:824–832.
9. Uhlenberg B, Schuelke M, Rüschendorf F, et al. Mutations in the gene encoding gap junction protein α12 (connexin 46.6) cause Pelizaeus-Merzbacher-like disease. Am J Hum Genet 2004;75:251–260.
10. Krabbe K, Nielsen JE, Fallentin E, et al. MRI of autosomal dominant pure spastic paraplegia. Neuroradiology 1997;39:724–727.
11. Dyck PJ, Giannini C, Lais A. Pathologic alterations of nerves. In: Dyck PJ, Thomas PK, Griffin JW, et al., eds. Peripheral neuropathy. 3rd ed. Philadelphia: WB Saunders, 1993:514–595.
12. Shaw CJ, Shaw CA, Yu W, et al. Comparative genomic hybridisation using a proximal 17p BAC/PAC array detects rearrangements responsible for four genomic disorders. J Med Genet 2004;41:113–119.
13. Griffiths I, Klugmann M, Anderson T, et al. Axonal swellings and degeneration in mice lacking the major proteolipid of myelin. Science 1998;280:1610–1613.
14. Anderson TJ, Schneider A, Barrie JA, et al. Late-onset neurodegeneration in mice with increased dosage of the proteolipid protein gene. J Comp Neurol 1998;394:506–519.
15. Garbern JY, Yool DA, Moore GJ, et al. Patients lacking the major CNS myelin protein, proteolipid protein 1, develop length-dependent axonal degeneration in the absence of demyelination and inflammation. Brain 2002;125:551–561.
16. Kleinjan DA, van Heyningen V. Long-range control of gene expression: emerging mechanisms and disruption in disease. Am J Hum Genet 2005;76:8–32.
17. Muncke N, Wogatzky BS, Breuning M, et al. Position effect on *PLP1* may cause a subset of Pelizaeus-Merzbacher disease symptoms. J Med Genet 2004;41:e121.
18. Churikov D, Siino J, Svetlova M, et al. Novel human testis-specific histone H2B encoded by the interrupted gene on the X chromosome. Genomics 2004;84:745–756.
19. Boespflug-Tanguy O, Giraud G, Mimault C, et al. Heterogeneous rearrangements of the PLP genomic region in Pelizaeus-Merzbacher Disease: genotype-phenotype correlation in 41 patients. Am J Hum Genet 1999;65(suppl):A285.
20. Velagaleti GVN, Bien-Willner GA, Northup JK, et al. Position effects due to chromosome breakpoints that map ~900 kb upstream and ~1.3 Mb downstream of *SOX9* in two patients with campomelic dysplasia. Am J Hum Genet 2005;76:652–662.
21. Woodward KJ, Cundall M, Sperle K, et al. Heterogeneous duplications in patients with Pelizaeus-Merzbacher disease suggest a mechanism of coupled homologous and nonhomologous recombination. Am J Hum Genet 2005;77:966–987.

Neuroscience 141 (2006) 1861–1869

ABERRANT TRAFFICKING OF A PROTEOLIPID PROTEIN IN A MILD PELIZAEUS-MERZBACHER DISEASE

S. KOIZUME,[a,c,d] S. TAKIZAWA,[a,c] K. FUJITA,[b] N. AIDA,[b] S. YAMASHITA,[a] Y. MIYAGI[d] AND H. OSAKA[a,c]*

[a]*Division of Neurology, Clinical Research Institute, Kanagawa Children's Medical Center, Mutsukawa 2-138-4, Minami-ku, Yokohama 232-8555, Japan*

[b]*Division of Radiology, Clinical Research Institute, Kanagawa Children's Medical Center, Yokohama 232-855, Japan*

[c]*Information and Cellular function, PRESTO, Japan Science and Technology Corporation, Kawaguchi, Saitama 332-0012, Japan*

[d]*Molecular Pathology and Genetics Division, Kanagawa Cancer Center Research Institute, Yokohama 241-0815, Japan*

Abstract—Pelizaeus-Merzbacher disease (PMD) is a rare X-linked leukodystrophy caused by proteolipid protein 1 (*PLP1*) gene mutations. Previous studies indicated that proteolipid proteins (PLPs) with disease-associated mutations are misfolded and trapped in the endoplasmic reticulum (ER) during transportation to the cell surface, which eventually leads to oligodendrocyte cell death in PMD. Here we report a PMD patient with a very mild phenotype carrying a novel mutation (485G→T) in exon 4 of the *PLP1* gene that causes a $Trp^{162}Leu$ substitution in the protein. We also investigated intracellular trafficking of this mutant PLP in COS-7 cells. Transiently transfected mutant PLP^{W162L} fused to an enhanced green fluorescent protein (EGFP) or a short peptide tag was not carried to the plasma membrane. However, in contrast to previous studies, this mutant PLP was not retained in the ER, indicating an escape of the newly translated protein from the quality control machinery. We also found that the mutant PLP accumulated in the nuclear envelope (NE) in a time-dependent manner. This mutant PLP, with its distribution outside the ER and a very mild phenotype, supports the idea that accumulation of misfolded mutant protein in the ER causes the severe phenotype of PMD.

Key words: Pelizaeus-Merzbacher disease, proteolipid protein, intracellular trafficking, unfolded protein response.

Pelizaeus-Merzbacher disease (PMD) and its allelic disorder, spastic paraplegia type 2, (SPG2) are X-linked recessive disorders associated with aberration of the proteolipid protein 1 (*PLP1*) gene. Proteolipid protein (PLP) is composed of 276 amino acid residues and predominantly expressed in oligodendrocytes of the CNS. As an integral membrane protein necessary for stabilization and maintenance of the myelin sheath (Inoue, 2005), it comprises up to ~50% of total myelin protein (Inoue, 2005). PMD is generally classified according to clinical or pathological features into mild (classical) or severe (connatal) forms (Griffiths et al., 1998; Inoue, 2005). A milder form of this disorder caused by mutations of the *PLP1* gene is known as spastic paraplegia (SPG) 2 (Griffiths et al., 1998; Inoue, 2005). Although the common feature of PMD is hypomyelination (Roussel et al., 1987; Schneider et al., 1992; Kagawa et al., 1994; Readhead et al., 1994) in the CNS, degeneration of oligodendrocytes is also characteristic in severe cases (Gow et al., 1998; Cerghet et al., 2001).

Various types of mutations of the *PLP1* gene, including exonic or intronic mutations, duplication, or deletion of the entire gene are responsible for PMD (Griffiths et al., 1998; Inoue, 2005). Patients carrying duplicated alleles show demyelination and patients with no *PLP1* alleles show only very mild clinical symptoms (Inoue, 2005), suggesting that the disease is caused by a toxic gain-of-function. It is known that exonic point mutations are present in 10~25% of reported PMD cases with variations in disease severity (Boespflug-Tanguy et al., 1994). DM20, an isoform of PLP whose role in the CNS is unclear, is produced from a *PLP1* transcript that lacks the second half of exon 3. Mutations in this region usually cause mild symptoms consistent with SPG. However, mutations in other coding regions of the *PLP1* gene usually cause severe mental retardation and deficits in motor function (i.e. loss of head control and sitting) with diffuse T2 elongation in magnetic resonance imaging (MRI) and disappearance of the II-V waves in auditory brain responses. Various intracellular trafficking studies have been conducted with the PLPs resulting from point mutations of the *PLP1* gene (Gow et al., 1994a,b; Thomson et al., 1997; Ghandour et al., 2002). Previous *in vitro* transfection studies in non-glial cells indicated that various mutant PLPs, irrespective of associated disease severity, are trapped in the endoplasmic reticulum (ER) immediately after translation, and thereby not transported to the plasma membrane (Gow et al., 1994b; Gow and Lazzarini, 1996; Thomson et al., 1997). Several studies have suggested that ER-retention of mutant PLP/DM20s causes oligodendrocytic programmed cell death (Gow et al., 1998; Cerghet et al., 2001; Southwood et al., 2002). An unfolded protein response (UPR) followed by caspase activation-mediated apoptosis is a plausible mechanism given the ER stress induced by accumulation of mutant

*Correspondence to: H. Osaka, Division of Neurology, Clinical Research Institute, Kanagawa Children's Medical Center, Mutsukawa 2-138-4, Minami-ku, Yokohama, 232–8555, Japan. Tel: +81-45-711-2351; fax: +81-45-721-3324.
E-mail address: kcmc_ho@cameo.plala.or.jp (H. Osaka).

Abbreviations: BiP, 78-kDa glucose regulated protein/immunoglobulin heavy chain binding protein; CFTR, cystic fibrosis transmembrane conductance regulator; DYT1 dystonia, torsion dystonia type 1; EGFP, enhanced green fluorescent protein; ER, endoplasmic reticulum; MRI, magnetic resonance imaging; NE, nuclear envelope; PLP, proteolipid protein; *PLP1 gene*, proteolipid protein 1 gene; PMD, Pelizaeus-Merzbacher disease; SPG, spastic paraplegia; UPR, unfolded protein response.

0306-4522/06$30.00+0.00
doi:10.1016/j.neuroscience.2006.05.067

PLP/DM20s in the ER (Gow and Sharma, 2003). In case of PMDs due to *PLP1*-gene duplication, demyelination is thought to be caused by perturbed protein transport such as impaired raft membrane trafficking (Simons et al., 2002). Involvement of UPR is unlikely because activation of caspase-12 was not detected in CNS of PLP-overexpressor mice (Cerghet et al., 2001).

In this study, we present a PMD patient with a very mild phenotype who could stand and speak a few words at 20 months, displayed almost complete myelination in both T1 and T2 images of MRI, and whose V waves were all detectable in auditory brain-stem response. We sequenced the patient's *PLP1* exons, and found a novel missense mutation in codon 162 (485G→T, $Trp^{162}Leu$). We further analyzed the effect of the mutation on trafficking of PLP in cells using confocal microscopy. In contrast to the results of previous studies, we found that PLP^{W162L} transiently expressed in COS-7 cells as a fusion protein of either enhanced green fluorescent protein (EGFP) or a FLAG peptide tag is not retained in the ER after synthesis and does not reach the cell surface. Furthermore, we found that PLP^{W162L}-EGFP accumulates in the nuclear envelope (NE). These data together with the very mild phenotype of our patient, similar to *PLP1*-null patients, support the idea that the UPR plays a crucial role in PMD.

EXPERIMENTAL PROCEDURES

Patient

This 3-year-old boy was born uneventfully at full term to unrelated Japanese parents. He was born with a body weight of 2990 g and an Apgar score of 9/9 at 1 and 5 min. No stridor or nystagmus was noted. He gained head control at 4 months, could sit without support at 14 months and could stand at 20 months, when he was referred to our hospital for evaluation of developmental delay. He could speak a few words and stand with support. Nystagmus was observed when he gazed laterally. He exhibited left hemiparesis with his upper extremities rotated inwardly and flexed at the elbow. His muscle tone was hypotonic with all extremities displaying exaggerated tendon reflexes and bilateral extensor plantar responses. No cerebellar signs or involuntary movements were observed. His developmental milestones were 9 months for motor function, 10 months for language understanding and 18 months for fine motor movements. Upon routine laboratory examination, no biochemical abnormalities were noted in serum ammonia, lactate and pyruvate levels, very long chain fatty acids and lysosomal enzymes. Myelin basic protein was not detected in the CSF. Nerve conduction velocities and electromyographic studies were all normal. Auditory brain-stem response elicited normal latencies with normal detectable V waves. MRI revealed a completion of myelination and a subependymal cyst in the right frontal region in the T1 signal. Myelination was incomplete in the insula and optic radiation in the T2 signal (Fig. 1).

Genomic DNA sequencing

Genomic DNA from this patient was prepared from white blood cells using the Wizard Genomic DNA purification kit (Promega, Madison, WI, USA). PCR of seven exons and promoter regions of the *PLP1* gene was performed as previously described (Osaka et al., 1999). Subsequent sequencing analyses of the PCR fragments were performed by direct sequencing using the Big Dye Terminators v1.1 Cycle Sequencing kit (Applied Biosystems, Foster City, CA, USA).

Cell culture and transfection

COS-7 cells were cultured in Dulbecco's modified Eagle's medium (DMEM) (Gibco BRL, Carlsbad, CA, USA) supplemented with 10% fetal bovine serum (Gibco BRL), 2 mM glutamine (Gibco BRL), and 100 U/ml penicillin/streptomycin (Gibco BRL) at 37 °C under humidified 5% CO_2 atmosphere. This cell line is non-glial in origin but does not express endogenous PLP and has often been used for intracellular trafficking studies of PLPs. Transient transfection of all plasmid constructs used in this study was performed using Lipofectamine™ 2000 (Invitrogen, Carlsbad, CA, USA) according to the manufacturer's protocol.

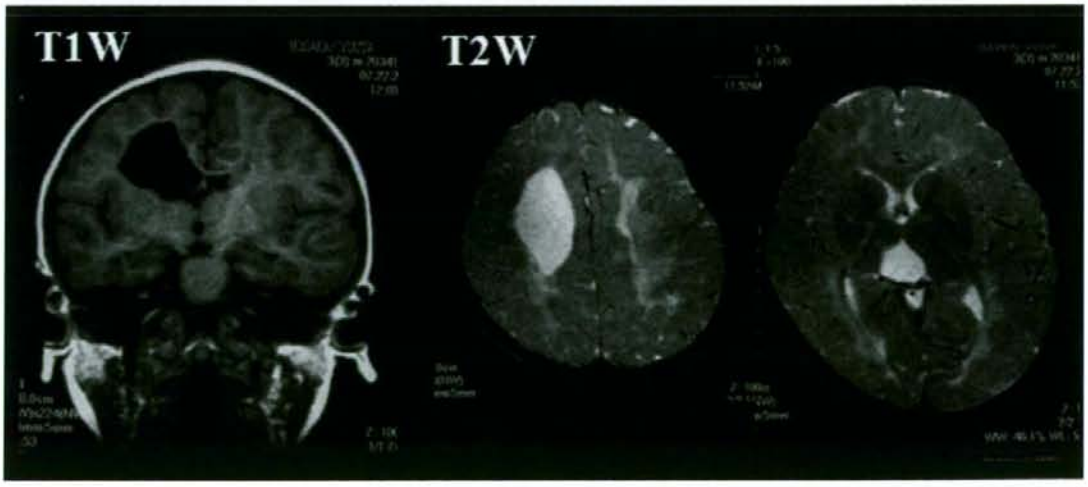

Fig. 1. Magnetic resonance images at two y. T1-weighted image shows a subependymal cyst in the right frontal region. Myelination is complete in the T1-weighted image. Myelination is incomplete in the optic radiation and internal capsule in the T2-weighted image.

Plasmid construction

Full-length cDNA of human *PLP1* (positions 119–949, accession no. M27110) was amplified by PCR and cloned into the pEGFP-N1 vector (Clontech, Mountain View, CA, USA) at the *EcoRI*/*BamHI* site to produce pPLP-EGFP. We took advantage of this vector, due to its strong gene expression driven by a CMV promoter, to recapitulate the high level of PLP expression in oligodendrocytes (Gow, 2003). PLP^{W162L} and its negative or positive ER retention controls, wild-type PLP (PLP^{WT}) and $Ala^{242}Val$ (myelin synthesis deficient) mutant PLP (PLP^{msd}), respectively, were designed to fuse to an EGFP at its C-terminal end for direct detection in live cells. A construct for expression of wild-type PLP fused to a FLAG tag was derived from $pPLP^{WT}$-EGFP. A plasmid was designed to express PLP-FLAGs by inserting a FLAG tag nucleotide sequence between the PLP and EGFP sequences and halting translation before synthesis of the EGFP moiety was initiated. A double-stranded oligonucleotide consisting of a FLAG sequence with a stop codon at the 3′-end was ligated into pPLP-EGFP at the *BamHI* site to produce pPLP-FLAG-EGFP. Bacterial colonies transformed by ligated plasmids with the desired FLAG sequence orientation were selected by colony PCR. The resulting plasmid constructs were propagated by standard procedures and purified using a QIA filter plasmid kit (Qiagen, Germantown, MD, USA). Site-directed mutagenesis of the pPLP-EGFP and pPLP-FLAG constructs was performed using a QuikChange™ site-directed mutagenesis kit (Stratagene, La Jolla, CA, USA) according to the manufacturer's protocol. Primers used for strand synthesis were 5′-CCTGACCGTTGTGTTGCTCCTGGTG-3′ and 5′-CACCAGGAGCAACACAACGGTCAGG-3′ (for the Trp162Leu conversion), and 5′-CCTGTTTATTGCTGTATTTGTGGGGG-3′ and 5′-CCCCCACAAATACAGCAATAAACAGG-3′ (for the Ala242Val conversion). Mutant plasmid constructs were confirmed by nucleotide sequencing using the BigDye™ Terminator Cycle Sequencing Ready Reaction kit (Applied Biosystems).

Analyses of subcellular localization of PLPs in living cells

Cultured cells, transfected with pPLP-EGFPs alone or with both pPLP-EGFP and pDsRed2-ER (Clontech), were directly examined for confocal microscopy. Subcellular localization of PLP-EGFPs was analyzed by laser scanning microscopy using a model LSM5 PASCAL system (Carl Zeiss Microimaging, Inc., Thornwood, NY, USA).

Immunofluorescence staining

Cells were seeded on four-well chamber glass slides (Falcon, Franklin Lakes, NJ, USA) and cultured for 20 or 40 h. After 20 h of transient transfection of pPLP-FLAGs or pPLP-EGFPs, cells were briefly washed once with PBS and fixed with 4% paraformaldehyde in PBS for 10 min. Fixed cells were washed twice with PBS and permeabilized with 0.1% Triton X-100 (Sigma, St. Louis, MO, USA) in PBS for 10 min. Cells were washed and incubated with 3% normal goat serum (Nichirei, Tokyo, Japan) for 15 min to reduce non-specific binding of antibodies and then incubated for 1 h with primary antibodies of anti-FLAG (1:100; F7425, Sigma), anti-KDEL (BiP, 78-kDa glucose regulated protein/immunoglobulin heavy chain binding protein) (1:100; SPA-827, Stressgen, Ann Arbor, MI, USA), or anti-laminA (1:100; sc-20680, Santa Cruz Biotechnology, Santa Cruz, CA, USA) diluted with blocking reagent containing 0.1% Triton X-100. After washing (10 min×3) with PBS, cells were finally incubated for 1 h with secondary antibodies conjugated with Alexa Fluor 488 or 546 dyes (Molecular Probes, Carlsbad, CA, USA) diluted with blocking reagent. Labeled cells were washed and sealed using the SlowFade® antifade kit (Molecular Probes). All steps were carried out at RT. Subcellular localization of proteins was analyzed by confocal microscopy as described above.

RESULTS

Sequencing of exons of the PLP1 gene and plasmid construction

By direct sequencing of the patient's *PLP1* gene exons and a promoter region, we found a novel missense mutation (485G→T, $Trp^{162}Leu$) in codon 162, in which another missense mutation (484T→C, $Trp^{162}Arg$) had been previously reported in a severe PMD patient (Hudson et al., 1989). No other sequence alterations were found and this mutation was not detected in more than 200 alleles. Furthermore, amino acid sequences are completely conserved within vertebrates and no protein polymorphism is known in the PLP (Inoue, 2005). Therefore, the $Trp^{162}Leu$ substitution appears to cause PMD. Previous transfection studies showed that all PLPs with a disease-associated point mutation were localized in the perinuclear ER, probably due to misfolding.

Subcellular localization of PLP^{W162L}-EGFP transiently expressed in COS-7 cells

We first estimated the subcellular localization of EGFP in COS-7 cells. After 40 h of transient cDNA transfection, non-fused EGFP was distributed within the cytoplasm including the nucleus of cells (Fig. 2A) as reported previously (Boucher et al., 2002). PLP^{WT}-EGFP was distributed throughout the cell body except the nucleus (Fig. 2B) and extended to the periphery of cells (Fig. 2B, arrows), suggesting insertion in the plasma membrane as previously shown by immunostaining of transfected HEK293 cells with a conformation specific O10 antibody (Boucher et al., 2002). We confirmed the extension of PLP^{WT}-EGFP to the cell surface by overlaying its fluorescence image with a light field micrograph (Fig. 3). PLP^{msd}-EGFP, as expected, accumulated in the perinuclear region in most cells and was not transported to the cell surface (Fig. 2C). PLP^{W162L}-EGFP also accumulated in the perinuclear region like the *msd* mutant but was not found at the cell periphery where the wild-type PLP was observed (Fig. 2D, arrowheads), suggesting that arrival at the cell surface is unlikely. The absence of PLP^{W162L}-EGFP in the plasma membrane was further confirmed by overlaying the fluorescence image with its light field micrograph (Fig. 3). In addition, a $Trp^{162}Leu$ mutant localization characteristic for that of the perinuclear rim was unexpectedly detected in many cells (Fig. 2D, arrows).

Subcellular localization of PLP^{W162L}-EGFP transiently co-expressed with DsRed2-ER

We performed time-lapse monitoring of the subcellular localization of wild-type and mutant PLP-EGFPs. As a marker for ER, we used the red-fluorescent DsRed2-ER protein, in which the ER retention signal peptide of calreticulin was anchored. After 15, 24, and 40 h of co-transfection with pPLP-EGFPs and pDsRed2-ER, presence of wild-type and mutant PLP-EGFPs in the ER was directly exam-

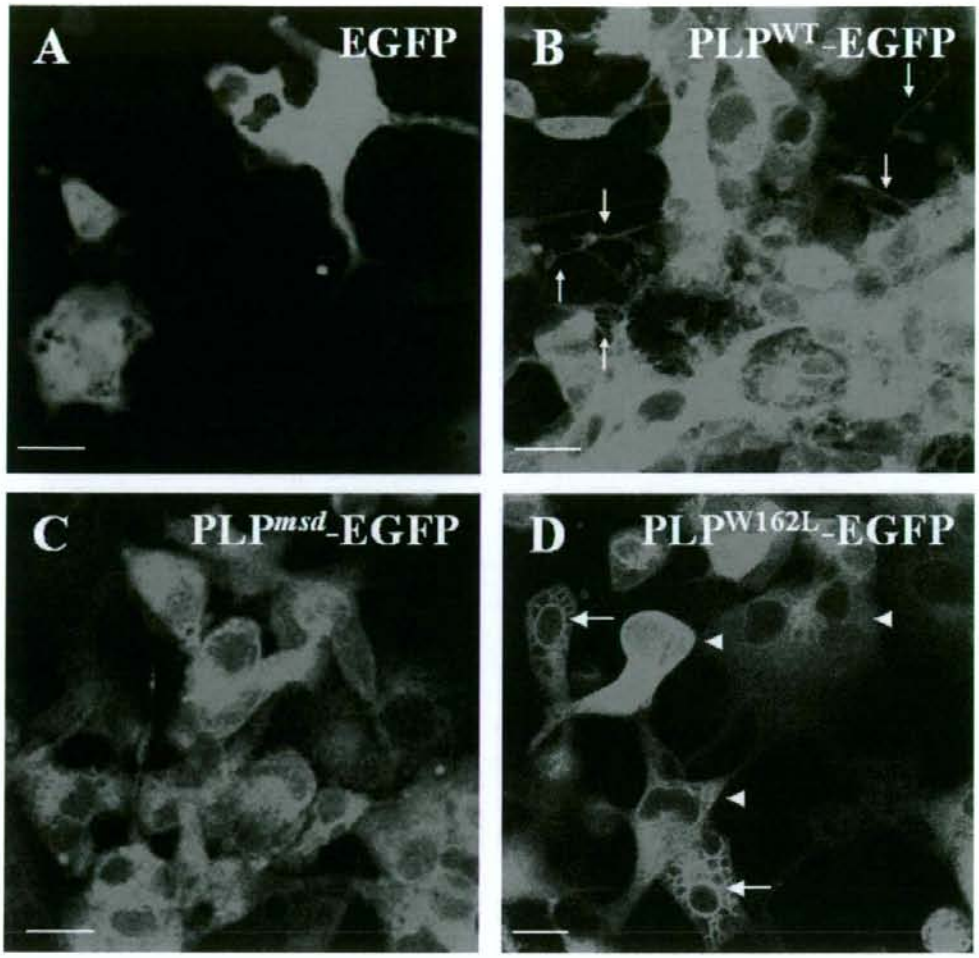

Fig. 2. Live-cell images of wild-type or mutant PLP-EGFPs transiently transfected in COS-7 cells. Confocal laser scanning images were collected 40 h after transfection with EGFP (A), PLP^{WT}-EGFP (B), PLP^{msd}-EGFP (C), or PLP^{W162L}-EGFP (D). Arrows in B are indicative of wild-type PLP-EGFP in the cell periphery. Arrowheads and arrows in D are indicative of PLP^{W162L}-EGFP localizations in the perinuclear region and at the perinuclear rim, respectively. Each panel is a representative, single optical slice image from independent, duplicate experiments. Scale bars=20 μm.

ined (Fig. 4). The negative control experiment revealed that EGFP alone did not colocalize with DsRed2-ER at 15 and 24 h (Fig. 4A) although some colocalization, seen as orange fluorescence, was detected at 40 h (Fig. 4A). Much of the PLP^{WT}-EGFP was found in the cytoplasmic region (Fig. 4B, green color around yellow colored region), suggesting that wild-type PLP passed through the ER and was transported to the cytoplasm. However, yellow fluorescence was found in the perinuclear regions of PLP^{WT}-EGFP transfected cells in the three time periods and is evidence that wild-type PLP was localized to the ER throughout the time course (Fig. 4B, arrows). In cells co-transfected with the positive ER-retention control PLP^{msd}-EGFP, the majority of the fluorescence is localized in the perinuclear region and is visible as a yellow color due to colocalization with the ER in most cells at all time points examined (Fig. 4C). Unlike the wild-type protein, we did not find much green fluorescing *msd* mutant protein *around* the ER, confirming its entrapment *in* the ER. These results also show that the overall characteristics of intracellular trafficking of both EGFP-tagged PLP^{WT} and PLP^{msd} are not altered throughout the time-course in COS-7 cells.

The PLP mutant, PLP^{W162L}-EGFP (green fluorescence) was found largely in cytoplasmic regions beyond the ER (Fig. 4D) at all time points. At 15 and 24 h post transfection, some PLP^{W162L}-EGFP was found in the ER (yellow fluorescence) (Fig. 4D, arrows). This suggests a passage of this mutant, similar to that of the wild-type protein, through the ER quality control mechanism. Surprisingly however, PLP^{W162L}-EGFP expressed 40 h after transfection did not overlap with, and was clearly distinct from, the ER in most cells (Fig. 4D and Supplement 1), but